DISCRIMINATION OF BEDFORM SCALES USING ROBUST SPLINE FILTERS AND WAVELET TRANSFORMS: METHODS AND APPLICATION TO SYNTHETIC SIGNALS AND THE RIO PARANA, ARGENTINA

by

Ronald R. Gutierrez

BSc, National University of Engineering, Peru, 1997

Submitted to the Graduate Faculty of

the Swanson School of Engineering in partial fulfillment

of the requirements for the degree of

Master of Science

University of Pittsburgh

2012

UNIVERSITY OF PITTSBURGH

SWANSON SCHOOL OF ENGINEERING

This thesis was presented

by

Ronald R. Gutierrez

It was defended on

March 28th, 2012

and approved by

Jorge D. Abad, PhD, Assistant Professor, Department of Civil and Environmental Engineering, University of Pittsburgh

Xu Liang, PhD,Associate Professor, Department of Civil and Environmental Engineering, University of Pittsburgh

Daniel Budny, PhD, Associate Professor, Department of Civil and Environmental Engineering, University of Pittsburgh

Piervincenzo Rizzo, PhD, Associate Professor, Department of Civil and Environmental Engineering, University of Pittsburgh

Eddy J. Langendoen, PhD, National Sedimentation Laboratory, USDA

Thesis Advisor: Jorge D. Abad, PhD, Assistant Professor, Department of Civil and Environmental Engineering, University of Pittsburgh

DISCRIMINATION OF BEDFORM SCALES USING ROBUST SPLINE FILTERS AND WAVELET TRANSFORMS: METHODS AND APPLICATION TO SYNTHETIC SIGNALS AND THE RIO PARANA, ARGENTINA

Ronald R. Gutierrez, MS

University of Pittsburgh, 2012

Currently, there is no standard nomenclature and procedure to systematically identify the scale and magnitude of bedforms such as bars, dunes and ripples that are commonly present in many sedimentary environments. This thesis proposes a standardization of the nomenclature and symbolic representation of bedforms, and details the combined application of robust spline filters and continuous wavelet transforms to discriminate these morphodynamic features, namely bedform hierarchies (BHs). The proposed methodology for bedform discrimination is applied to synthetic bedform signals, which are sampled at a Nyquist ratio interval of 5 to 100 and a signal-to-noise ratio interval of 1 to 20, and to a detailed 3D bed survey of the Rio Parana, Argentina, which exhibits large-scale dune bedforms with superimposed, smaller bedforms. After discriminating the synthetic bedform signals into 3 BHs that represent bars, dunes and ripples, the accuracy of the methodology is quantified by estimating the reproducibility, the cross correlation and the standard deviation ratio of the actual and retrieved signals. For the case of the field measurements, the proposed method is used to discriminate small and large dunes; and subsequently, obtain and statistically analyze the common morphological descriptors such as wavelength, slope, and amplitude for both stoss and lee sides of these different size bedforms. The analysis of the synthetic signals demonstrates that the Morlet wavelet function is the most efficient in retrieving smaller periodicities such as ripples and that the proposed methodology effectively discriminate the

waves of different periodicities scales for Nyquist ratios higher than 50 and signal-to-noise ratios. The analysis of the bedforms of the Parana River reveals that in most cases, a Gamma probability distribution (with a positive skewness) best describes the dimensionless wavelength and amplitude for both the lee and stoss sides of large dunes. For the case of the smaller superimposed dunes, the dimensionless wavelength shows a discrete behavior governed by the sampling frequency of the data, and the dimensionless amplitude better fits the Gamma probability distribution, again with a positive skewness.

TABLE OF CONTENTS

LIST OF TABLES

LIST OF FIGURES

PREFACE

To my mother, my brothers and sisters, and my beloved wife (for all their support and affection) with love and music

Ut queant laxis resonare fibris
Mira gestorum famuli tuorum,
Solve polluti labii reatum,
Sancte Iohannes.

ACKNOWLEDGEMENT

All my gratitude to Dr. Jorge D. Abad for his comments and encouragement. Special thanks to Dr. Jim Best and Dr. Dan Parsons.

1.0 INTRODUCTION

The morphology and dynamics of alluvial bedforms are strongly governed by the interrelationship between sediment transport and the hydraulic conditions. The persistent variability in the geometry and migration rates of bedforms in rivers is not an exception, but rather the hallmark of natural bedforms developing under, and interacting with, unidirectional shear flows [37]. However, at present we lack a consistent, non-arbitrary, quantitative description of both the morphology and dynamics that is necessary to understand and establish the effect bedform morphology has on bedform migration, sediment transport and the resultant bed roughness.

For the case of erodible channels with beds composed of non-cohesive materials, theoretical research on the morphodynamics of bedforms has largely followed five distinctive approaches: 1) where sediment continuity is incorporated into the hydraulic and sediment transport equations; 2) where instability of a water-bed interface is regarded as a Kelvin-Helmholtz type of instability between stratified layer of fluids; 3) where stability of a sinusoidal fluid-bed interface is investigated using linear stability theory; 4) where kinematically-admissible bedform profiles, containing stationary eddies in their lee side, were obtained using the Helmholtz-Kirchoff method of streamline prediction, and 5) where statistical correlations between dimensionless parameters are obtained through regression analysis [29].

Statistical methods developed for the description of sand waves in alluvial rivers were first proposed by Nordin and Algert [60] and Engelund and Fredsøe [21]. Research performed following the fifth approach outline above have typically used morphometric parameters such as bedform height (Δ), wavelength (λ) and steepness (Δ/λ) to describe and classify bedform features such as ripples and dunes commonly found on continental shelves and within river channels in various superimposed states [6, 17].

Some early studies considered bedform profiles to be stochastic variables [61, 35, 54] that were analyzed by using time series analysis techniques [51]. However, more recent studies have used a spatial scaling techniques that treat bed elevations in a bedform profile as a random function, rather than identifying individual bedforms in a profile [58, 37, 78]

It has been argued that ripples and dunes form two distinct populations and that distinct boundary layer regions are present on the stoss side of large dunes that are responsible for the ripple instability that generates superposed secondary forms [Jerolmack et al., 2006]. In terms of the Shields parameter θ, dunes form at larger values of θ, whereas ripples form at smaller values of θ. At intermediate values of θ, these two bedform features may coexist [28]

Field and laboratory research show that for both nonuniform and unsteady flows, bedforms have a minimum relaxation time in which they are able to equilibrate to a new hydraulic condition [3, 38, 57, 41, 10, 32] . Generally, both bedform height and wavelength increase with flow velocity, presenting both negative and positive hysteresis [27]. More recent work, based on experimental studies under steady flow conditions [50], found that scour in the dune trough is the main mechanism by which dunes increase in height, contrary to the common assumption that dunes grow by accretion or amalgamation.

Ripples show two-dimensional (2D) and three-dimensional (3D) patterns depending on their relative location on dunes and the hydraulic properties and patterns. Baas [7] demonstrated that ripples evolve from incipient, through straight, sinuous and non equilibrium linguoid, to equilibrium linguoid plan morphology. The transition time is related to an inverse power of the flow velocity, ranges from several minutes to several hours, and several days in some cases [81]. Venditti and his collaborators also point out that the reason why 3D bedforms are observed to exist in the upper part of the stability fields may simply be that it takes less time for the higher flow rate to move the sediment required for the transition. Usually, 3D ripple patterns are observed among dune troughs and crests although predominantly near to the crests. Likewise, dunes show 3D patterns that are intimately linked to the morphology of the upstream dune, with changes in crest line curvature and crest line bifurcations-junctions significantly influencing the downstream dune form [65].

Dunes are related to depositional histories and, similarly to ripples, are controlled by local hydraulic conditions such as changes in water depth, sediment flow rate and flow competence

[6]. Bars constitute an obvious source of non-stationarity of bedform signals that threaten to invalidate the spectral analysis of bedforms [5].

The variability of bedform is closely related to the total form roughness of a channel, and there is theoretical, laboratory, and field evidence that the roughness of all wave lengths exists up to the scales of the largest bedforms [36]. It has also been hypothesized that the variability in geometric variables of individual bedforms within a reach affects the reach-averaged form roughness [78].

Based on experimental measurements and field data, Yalin and Lai [85] proposed that (with reference to Figure 2.4a) the form resistance, f", when ripples are superimposed upon dunes can be estimated as $f" = 4\Xi$ if $\Xi > \simeq 10^{-2}$, and as $f" = [3.3\log(\Xi - 1) - 2.3]^{-2}$ if $\Xi < \simeq 10^{-2}$; where $\Xi = \frac{\Delta^2}{\Lambda h}$. These relationships suggest that drag resistance is dependent just on the geometric characteristics of dunes. Moreover, van der Mark et al. [78] hypothesize that the variability of individual bedforms within a reach affects the reach-averaged form roughness, and base this hypothesis on the analogy between grain roughness and form roughness. For example, the 65%, 84%, or 90% percentiles of the grain size distribution are often used as a representative particle diameter in predicting the grain roughness. Similarly, form roughness may also be determined from bedforms that are higher, longer or steeper than the median or mean bedform height, bedform length, or bedform steepness, respectively.

The quantification of variability in bedform geometry is necessary for scientific and practical purposes. For the former purpose, it is necessary for modeling: 1) bed roughness [76, 1], 2) the formation of cross-strata [11], 3) the vertical sorting of sediments [12, 48], 4) sediment transport rates [31, 71, 20, 47], 5) the transition between 2D and 3D dunes [81], and 6) velocity pulsations within the flow [30, 32]. Such quantification is also required for numerical modeling of flow over bedforms (e.g. [43, 82, 72]), assessing the interaction between flow over bedforms and ground-water [15, 14, 16], and evaluating contaminant transport [64]. For practical purposes, the study of the variability of bedforms is important in the prediction of floods and flow resistance [5, 39, 66, 44, 42, 26, 83], prediction of potential disturbance to man-made structures such as river tunnels [4], to predict future changes in sediment transport rates and biotic responses following dam removal [55], to estimate the relationship between bedform characteristics and biota [84, 73], and in river restoration projects [34].

Past approaches to the quantification of bedform variability have used and applied spectral analysis [35, 5, 51, 44], smoothing techniques such as a moving-average [78], signal roughness techniques [71], fractals [84], and logistic regression [40]. However, moving-average techniques as well as Fourier series analysis have generally proved to be insufficient as a tool to extract smooth curves from data [74]. This lack of success is primarily because in using spectral analysis, the mayor assumption is that the bedform waves are two-dimensional and not highly variable in the cross-stream direction [51]. Likewise, Fourier transform techniques, which are used in spectral analysis, has severe limitations when analyzing signals that include significant departures from stationarity and consist of intermittent and/or aperiodic processes. A high number of Fourier coefficients are then necessary to take these features into account, and which may be visible on some intervals but not in others [49]. This results in a limited representation of the frequencies of nonlinear processes such as river bed morphology.

Wavelet transforms (WT) were developed to overcome these limitations of the Fourier transforms. WT have been applied to fluid mechanics in the isolation of coherent structures in turbulent flows, in analyzing the temporal variability of coherent convective storm structures, within investigation of long-term land temperature/climate series, and in analyzing oxygen isotopic ratios from marine sediments [49].

Some recent applications of 1D-wavelets in sedimentology encompass temporal variations within streamflow and sediment loads [69], characterization of bedform morphology [17], sediment concentration distributions [22], the recognition of patterns in seabed morphology [52], analysis of riverbed roughness [62], and investigation of flow structure over alluvial sand dunes [70]. I demonstrate that this technique identifies the various scales of bedforms present within a series and significantly improves the quantification of form roughness at different bedform scales.

2.0 BEDFORM DISCRIMINATION METHOD AND FIELD STUDY SITE

2.1 DATA

2.1.1 Paraná Study Reach

The Rio Paraná River ranks among the Worlds largest rivers and has the fifth largest drainage area and seventh highest mean flow discharge of all rivers [27]. The study reach is located at 16 km north of Corrientes, NE Argentina (see Figure 2.1), close to its confluence with the Rio Paraguay. At the confluence, the annual discharge of the Rio Paraná increases from 11,983 to 16,941 $m^3 s^{-1}$ and the suspended sediment discharge from $5.1x10^6$ to $118.7x10^6$ tons $year^{-1}$. The climate at the study reach is subtropical with a mean annual temperature of 21.3 °C and a mean annual rainfall of 1,290 mm.

The flow regime of the Rio Paraná is characterized by summer floods (between February and March) and spring low water levels [63]. At the study reach, the channel pattern can be classified as multi thread/braided [63] and is approximately 2.5 km wide and 5-12 meters deep [65]. Parsons et al. [65], surveyed the river bed at the study reach using a RESON 8125 multibeam echo sounder, and simultaneously obtained 3D flow information with an acoustic Doppler current profiler. Therefore, a bed area of continuous morphological data with a 370-m width and 1.028-km length area was obtained. In order to prepare the data for the present analysis, a structured 1-m grid was obtained from this survey. Thus, 370 longitudinal transects of 1028 points (1-m sampling frequency and NR=100) were obtained. The first transect (j=1) was located at the northing 6977640 and the last (j=370) at the northing 6978010 (Figure 2.2). Figure 2.2 also shows that the bed morphology of the Paraná River is characterized by 3D dunes with few straight crests that are subparallel, but with

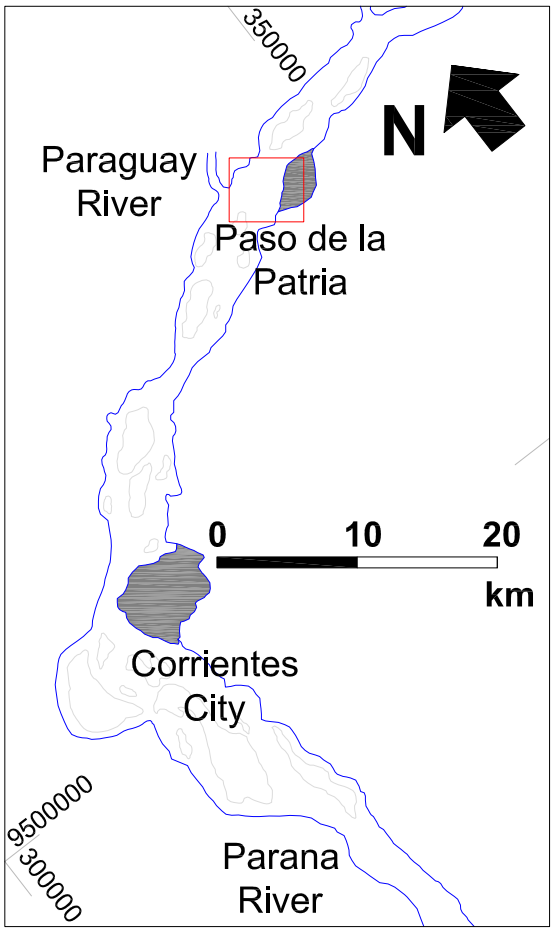

Figure 2.1: Study reach location of Paraná River

numerous undulating crests with saddles and lobes which occasionally bifurcate, especially in regions of deeper flow [65]. Inspection of the transects at the center and boundaries of the survey area (see Figure 2.3) shows that most of the dunes are highly asymmetric, with crestal platforms followed by marked changes of slope on the lee side (see [65] for more details).

2.1.2 Synthetic Data

In order to assess the accuracy of the proposed discrimination methodology, a set of synthetic signals are produced. These signals are comprised by three layers of waves of different periodicity scales intended to replicate ripples, dunes and bars. Bars are represented by the sinusoidal function $\eta_3(x) = a * Sin(2x/T - c) + d$; where x is the relative distance in meters, $a = 0.05$ m, T (the period) is equal to 200, $c = 100$ and $d = 0.05x$. The term d provides for a slope in the bar synthetic signal. The stoss side of the dunes are represented by the lower-regime dunes equation $\eta_{2,s}(x)$ defined by Equation 2.1 and proposed by Haque and Mahmood [29]. The lee face is represented by a straight line, and defined by Equation 2.2.

$$\eta_{2,s} = SL\left\{\frac{1}{2\pi \sin\frac{k\pi}{2}}\left(\ln\sin\frac{\pi}{L}\left(x + \frac{L}{2}[1-k]\right) - \ln\sin\frac{\pi}{2}[1-k]\right) + \frac{x}{L}\right\}; \text{ for } 0 \leq x \leq kL \tag{2.1}$$

$$\eta_{2,l} = -\frac{a(L-x)}{(k-1)L}; \text{ for } kL < x \leq L \tag{2.2}$$

Where S is the wedge slope a/b, $S = tan(\theta)$, for θ =10 ° (see [29] for geometric details). L is the dune wavelength assumed to be equal to 10 m. k is the normalized length of the stoss face, which was assumed to be equal to 0.7. This value is close to $k = 0.667$ predicted by the theory for mature ripples and dunes [29]. Centered versions of these dunes are used in the present application. Ripples are represented by a random signal generated by using the Wichman-Hill algorithm. The mean of these signals is equal to zero; their variances were varied in order to obtain an interval of signal-to-noise ratios from 1 to 20, approximately. The signal-to-noise ratio (SNR) is defined as the ratio between the variance of the random signal and the variance of the signal comprised by the summation of the bar and dunes signals.

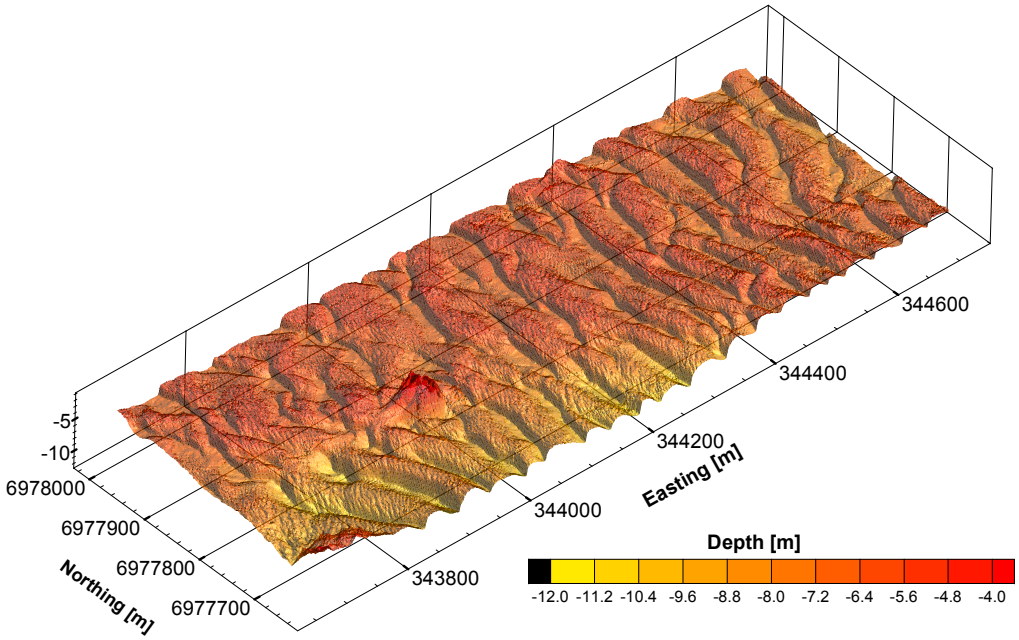

Figure 2.2: Bed morphology of the Paraná River after Parson et. al., 2005 [65]

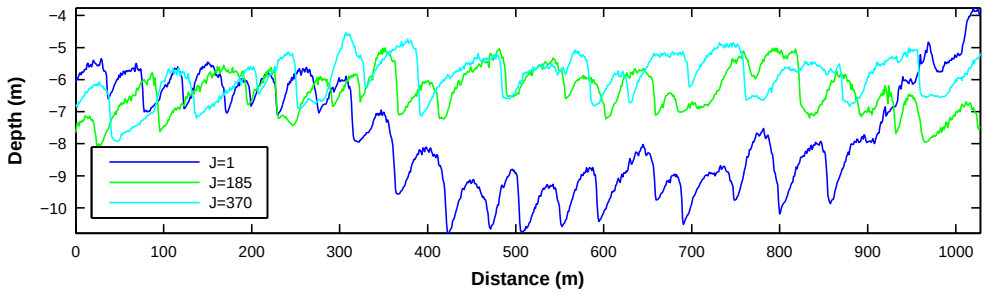

Figure 2.3: Bedform profiles from Figure 2.2

The signals are sampled at sample frequencies of 2m, 1m, 0.5m, 0.167m, 0.125m and 0.1m. Thus, an interval of Nyquist ratios (NRs) of 5, 10, 20, 60, 80 and 100 is obtained.

2.2 THE HIERARCHICAL SCALE DISCRIMINATION OF BEDFORMS

There is currently no standard definition nor methodology for the identification and discrimination of the different scales of bedforms (e.g. ripples, dunes, bars) generated on a natural mobile bed. As illustrated in Figure 2.4, various researchers have followed different approaches to quantify and name the geometric characteristics of bedforms. For example, bedform length has variously been defined as: 1) the length of a line connecting two subsequent troughs, 2) the distance between two successive mean bed level up-crossings, 3) the distance between two successive mean down-crossings, and 4) the distance of two successive crests or two successive troughs (see Figures 2.4c, 2.4f and 2.4h. Similarly, bedform height has been defined as either the distance between a crest and its downstream trough, or as the shortest distance between a crest and the line between two troughs [77]. Likewise, some researchers (Figures 2.4d and 2.4f) have discriminated the length and amplitude of both the lee and stoss sides of dunes, which is necessary because they represent markedly different regions of flow over asymmetrical dunes. In the lee side, a region of flow separation, with reattachment occurring approximately 4-8 dune heights downstream of the crest, and an expanding flow region are formed [70]. On the other hand, on the stoss side, a new internal boundary layer grows as flow re-establishes itself and develops a more logarithmic velocity profile [10].These same gross patterns of flow also exist over the stoss and lee sides of the ripples, although dunes both influence the water surface elevation and generate large-scale macroturbuelnce that may reach the water surface [8, 9, 68].

Scaling remains a characteristic signature of bedforms [1],and both field and laboratory data often show multiple superimposed scales of bedforms. It is therefore often necessary to effectively subdivide these differing bedform scales into useful, quantified waveforms with different periodicities. Ashley [6] proposed arbitrary thresholds of 5, 10, 100 m for bedform length to differentiate "small", "medium" and "large" dunes, and proposed a classification

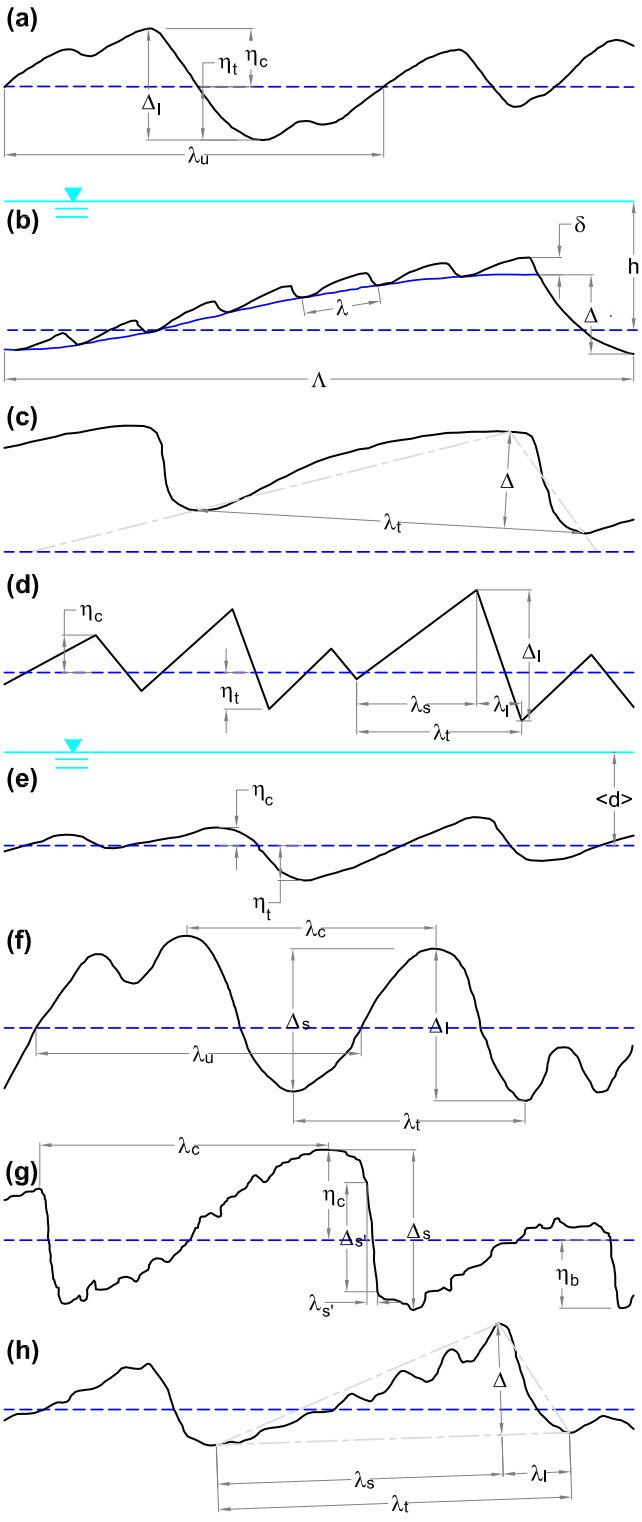

Figure 2.4: Bedform parameters

scheme to distinguish ripples from dunes by defining ripples as entities that have lengths generally less than 0.6 m. Although this criterion is based on an observational gap (which is currently being filled), it often used as an accepted criterion for distinguishing between ripples and dunes, but without any theoretical, or causative process explanation. In practice, the discrimination between ripples and dunes is often taken as obvious, so that many authors fail to explain the criteria used for their discrimination in field and laboratory studies [36]. It is clear that the study of differing scales of bedforms requires both a uniform method for their quantification and description of their geometric descriptors.

The most widely-used definitions of various bedform geometric descriptors are given in Figures 2.4a, 2.4b, 2.4d, 2.4e and 2.4f, with the definitions in Figures 2.4c and 2.4h often not being used [79]. It is important to note that the difference in the values of wavelength obtained between these different methods is minimal and can be neglected. In order to standardize the symbolic representation of bedform geometric descriptors, the symbols presented in Figure 2.5 are adopted herein. Many of these symbols have been widely used in past research, although they have not been used on a standardized basis (see Figure 2.4). Each descriptor is represented by a letter e.g. η (for bedform elevation), λ (for bedform length), Δ (for bedform height), and h (for water depth) followed by three indicators that represent [1] its position (as superscript, but avoiding this descriptor if the bedform elevation is represented) e.g. crest (c), trough (b), stoss (s), and lee (l); [2] its ordinal respect to all the hierarchies (as sub-script and giving the first ordinal to ripples); and [3] the total number of hierarchies (as a subscript). Therefore, the first hierarchy corresponds to the ripples, the second to the dunes, and the third to bars. Thus, for h (or η) the following relationship is always verified: $h = h_{1,3} + h_{2,3} + h_{3,3}$.

2.3 METHOD OF BEDFORM SCALE DISCRIMINATION

Investigations into bedform dynamics face the difficulty of defining an objective methodology to adequately quantify bedforms of different scale. This difficulty is principally due to the deterministic and stochastic nature of bedforms, where bedform profiles (BFPs) can

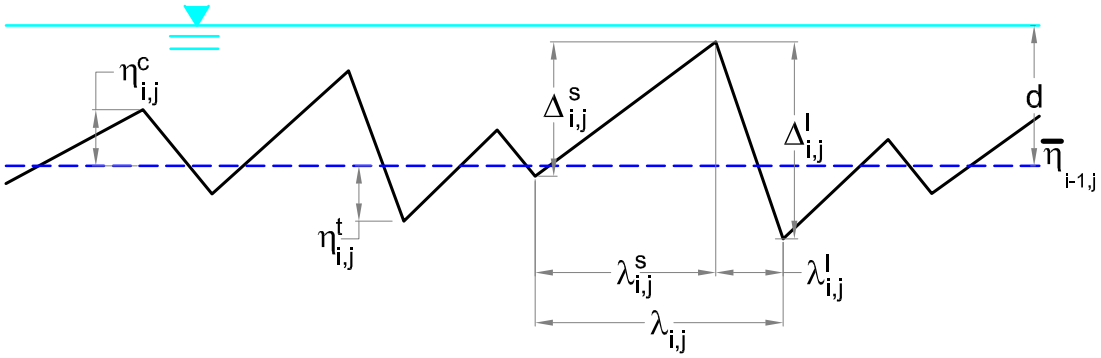

Figure 2.5: Symbolic representation of bedform descriptors for a given hierarchy adopted in the present contribution.

further be viewed as series of discrete bedform elements, continuous bed-elevation fields or some combination of these perspectives [18]. One of the latest studies of bedform discrimination was conducted by van der Mark et al. [79], who proposed a methodology named the bedform tracking tool (BTT) which uses spectral analysis and a weighted moving-average as a smoothing technique over BFPs that were previously verified to be statistically homogeneous. Generally speaking, the BTT works according to the following procedure over individual BFPs: [1] it finds and replaces outliers, [2] a trend line is estimated based on the nature of the BFP (e.g. flume experiments or field measurements), [3] the BFP is detrended, [4] the BFP is filtered by applying a weighted moving-average filter, [5] the zero upcrossings (points where the filtered BFP crosses the zero line) and downcrossings (point where the filtered BFP crosses the zero line in downward direction) shown in Figure 2.4g are obtained, and finally [6] the geometric characteristics of individual bedforms are estimated. This methodology performs reasonably well in minimizing any subjectivity in the estimation of the variability of bedforms, although it uses a filter that may not be completely suitable to detrend a BFP. A weighted-average is any average that has multiplying factors to give

different weights to data at different positions in the sample window. Mathematically, the moving-average is a convolution of the data points with a fixed weighting function, and can therefore be considered as a rigid convolution function. The present work proposes the use of robust spline filters and the application of continuous wavelet transforms to perform a hierarchical discrimination and separation of different bedform scales. Discrete wavelet transforms and robust spline filters have been successfully used in the discrimination of engineering surfaces [67], which similar to bedforms are comprised of a range of spatial wavelengths. Engineering surfaces are split into form profiles that are similar to bars, waviness profiles that are similar to dunes and roughness profiles that are similar to ripples.

2.3.1 The Robust Spline Filter

A fully automated robust spline procedure for uniformly-sampled datasets is used herein. The algorithm, based on a penalized least squares method, allows fast smoothing of uniformly sampled data y_i of n elements, by means of the discrete cosine transform. To minimize or cancel the side effects of high leverage (a measure of the influence, between 0 and 1, of a given point on a fitting model due to its location in the space of the inputs), the algorithm constructs weights with a specified weighting function by using the current residuals and updating them, from iteration to iteration, until the residuals remain unchanged. In practice, five iterative steps are sufficient [25]. The algorithm uses the bisquare weighting function that is mathematically defined by Equation (2.3). The smoothed data $\hat{y}_i$ is estimated by the parameter s which is a real positive scalar that controls the degree of smoothing: as the smoothing parameter increases, the smoothing of $\hat{y}_i$ also increases.

$$w_i = \begin{cases} rl\left[1 - \left(\frac{u_i}{4.685}\right)^2\right]^2 & \text{if } \left|\frac{u_i}{4.685}\right| < 1, \\ 0 & \text{if } \left|\frac{u_i}{4.685}\right| \geq 1 \end{cases} \tag{2.3}$$

where u_i is the Studentized residual which is adjusted for standard deviation and leverage and is mathematically represented by Equation (2.4).

$$u_i = \frac{r_i}{\hat{\sigma}\sqrt{1 - h_i}} \tag{2.4}$$

In the above equation $r_i = y_i - \hat{y}_i$ is the residual of the ith observation, h_i is its corresponding leverage and $\hat{\sigma}$ is a robust estimate for the standard deviation of the residuals given by 1.4826MAD, where MAD denotes the median absolute deviation. The leverage values h_i are all given by the diagonal elements of the hat matrix H. However, a faster and more economical alternative for robust smoothing can be obtained using an average leverage, which is mathematically defined by:

$$h_i = \frac{1}{n}\sum_i H_{ii} = \frac{Tr(H)}{n} \tag{2.5}$$

An approximated value for $Tr(H)/n$ is given:

$$\frac{Tr(H)}{n} \approx r_i \sum_{i=1}^{n} [1 + s(2 - 2\cos((i-1)\pi/n)^2]^{-1} \tag{2.6}$$

The approximated Studentized residuals finally reduce to the expression:

$$u_i = r_i \left| 1.4826\text{MAD}(r) \sqrt{1 - \frac{\sqrt{1+\sqrt{1+16s}}}{\sqrt{2}\sqrt{1+16s}}} \right|^{-1} \tag{2.7}$$

The use of the bisquare weightings in combination with the approximated Studentized residuals provides a robust version of the above-mentioned smoothing. An iteratively weighted robust version of the algorithm is used to deal with occurrences of missing and outlying values [25].

2.3.2 The Wavelet Transform

The unidimensional wavelet transform (WT) of a signal $f(x) \in L_2$ is obtained by the convolution of the signal and the wavelet function (WF) or mother wavelet $\psi(x)$ as expressed by Equation (2.8), where a is the scale parameter, b is the location parameter and $\bar{\psi}_{a,b}(t)$ is the complex conjugate of $\psi_{a,b}(t)$, as mathematically represented by Equation (2.9).

$$T(a,b) = \int_{-\infty}^{\infty} x(t)\bar{\psi}_{a,b}(t)\, dt, \text{ for } a > 0, \tag{2.8}$$

$$\psi_{a,b}(t) = \frac{1}{\sqrt{a}}\psi(\frac{t-b}{a}) \tag{2.9}$$

According to the Parseval's theorem the same wavelet transform can be expressed as:

$$T(a,b) = \frac{1}{2\pi}\int_{-\infty}^{\infty} \hat{x}(f)\bar{\hat{\psi}}_{a,b}(f)\, df \tag{2.10}$$

Where $\hat{x}(f)$ and $\hat{\psi}_{a,b}(f)$ are the Fourier transforms of $x(f)$ and $\psi_{a,b}(f)$, respectively. The wavelet power spectrum is defined as $|T(a,b)|^2$.

Wavelets have advantages over traditional Fourier methods in analyzing physical situations where the signal contains discontinuities and sharp spikes. They also provide a flexible time or spatial-scale window that is localized on time or space-scale planes [67]. The most widely-used continuous WFs are the Morlet and the $n-th$ derivatives of the Gaussian (DOG). Among the DOGs, the Ricker or so- called Mexican hat wavelet represents the second derivative. The selection of the appropriate WF depends on both the mathematical and physical nature of the parameter being analyzed. Different categories of wavelet, and various types of wavelets within each category, provide a multitude of options to choose from when analyzing a process of interest [23].

The complex Morlet function is expressed by Equation (2.11) in its simplest form (where k_0 is the central frequency, which is generally assumed to be 5 or bigger to satisfy the wavelet admissibility condition). The Ricker function, which is a real function, is mathematically represented by equation Equation (2.12).

$$\psi(t) = \frac{1}{\pi^{1/4}}.e^{i2\pi k_0 t}e^{-t^2/2} \tag{2.11}$$

$$\psi(t) = (1-t^2).e^{-t^2/2} \tag{2.12}$$

According to the uncertainty Heisenbergs principle, there is a lower limit to the product of frequency and time resolution. Thus, as time resolution is improved, frequency resolution degrades and vice versa [2]

The Morlet function provides lower area of the Heisenberg cell than the DOGs WT and retrieves accurate wavelengths at higher signal-to-noise ratios and lower sample frequencies.

The wavelet analysis of the synthetic signals confirms this. Morlet WF (see Figure 2.6) retrieves frequencies of the order of ripples for sampling frequencies below 0.25 m, and that the efficiency of the DOGs improves as the order of the derivative is increased. This efficiency of the Morlet WT is particularly important to retrieve frequencies of the order of ripples. Therefore, it is used for all the estimations with wavelet transforms. They are performed by using a modified version of the wavelet software provided by [75].

For each synthetic signal and Paraná River's BFP, the separation procedure encompasses the following steps and is valid for either h or η signals:

1. The outliers are identified and replaced by the mean water depth h (or bedform elevation η).
2. The continuous wavelet analysis is performed on the given h (or η) signal (see Figures 2.7 and 2.8). The global wavelet transform spectrum (see Figure 2.7c and 2.8c) provides information to find the wavelength (192 m for signal SSNR80SNR489 and 337 m for j=100) of the wave that underlies the dunes that have a mean wavelength of approximately 10 m and 62 m, respectively.
3. The original synthetic signal (η in Figure 2.9) and BFP (h in Figure 2.10) are filtered by using the spline robust filter with several values of the parameter s. A wavelet transform analysis is performed for each filtered signal and the one that has a mean wavelength close to 192 m (for SSNR80SNR489) or 337 m (for j=100) is found. These signals become the third level of the bedform discrimination ($h_{3,3}$ in Figure 2.10 and $\eta_{3,3}$ in Figure 2.9).
4. $\hat{h}_3$ (or $\hat{\eta}_3$ for the synthetic signals) is defined as $\hat{h}_3 = h - h_{3,3}$ and contains the signal of dunes with superimposed smaller dunes (or superimposed ripples, for the synthetic signals).
5. The $\hat{h}_3$ signal (or $\hat{\eta}_3$ for the synthetic signals) is filtered by using the robust spline filter with different values of the parameter s to obtain several dune-like signals, named $\hat{h}_2(s)$. For the case of synthetic signals several ripple-like signals, named $\hat{\eta}_2(s)$ are obtained.
6. The $\hat{h}_3$ signal is subtracted from each $\hat{h}_2(s)$ to obtain a set of smaller-dune-like signals, named $\hat{h}_1(s)$ (or ripple-like signals, named $\hat{\eta}_1(s)$ for the synthetic signals).
7. A wavelet analysis is performed on each $\hat{h}_1(s)$ and this determines a mean wavelength of 0.6 m (threshold that defines ripples) and 5m (threshold that defines small dunes)

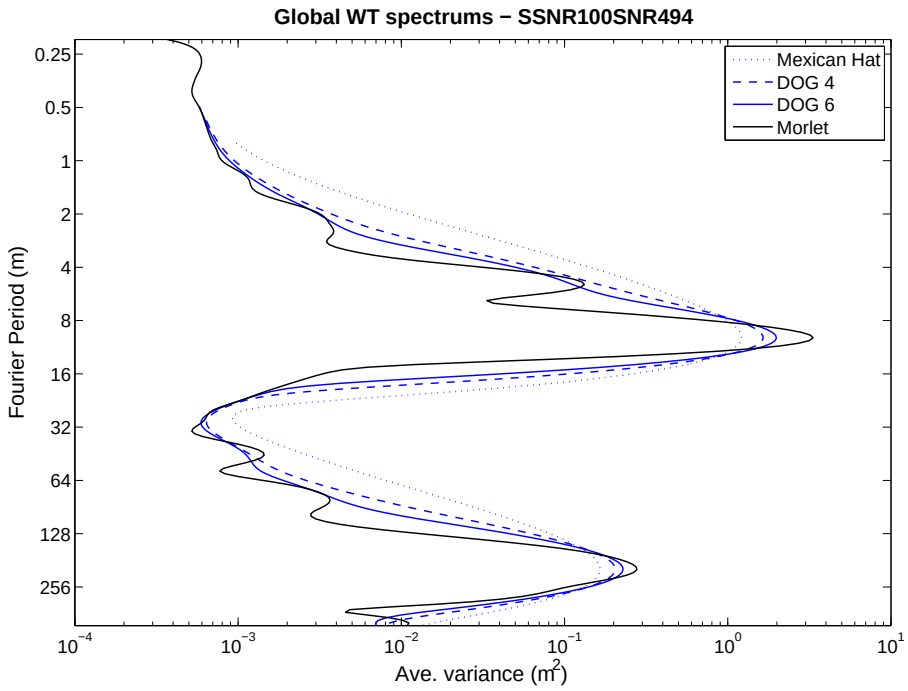

Figure 2.6: Wavelet global spectrum for Morlet and DOGs WF. The former retrieves higher frequencies at any SNR and NR.

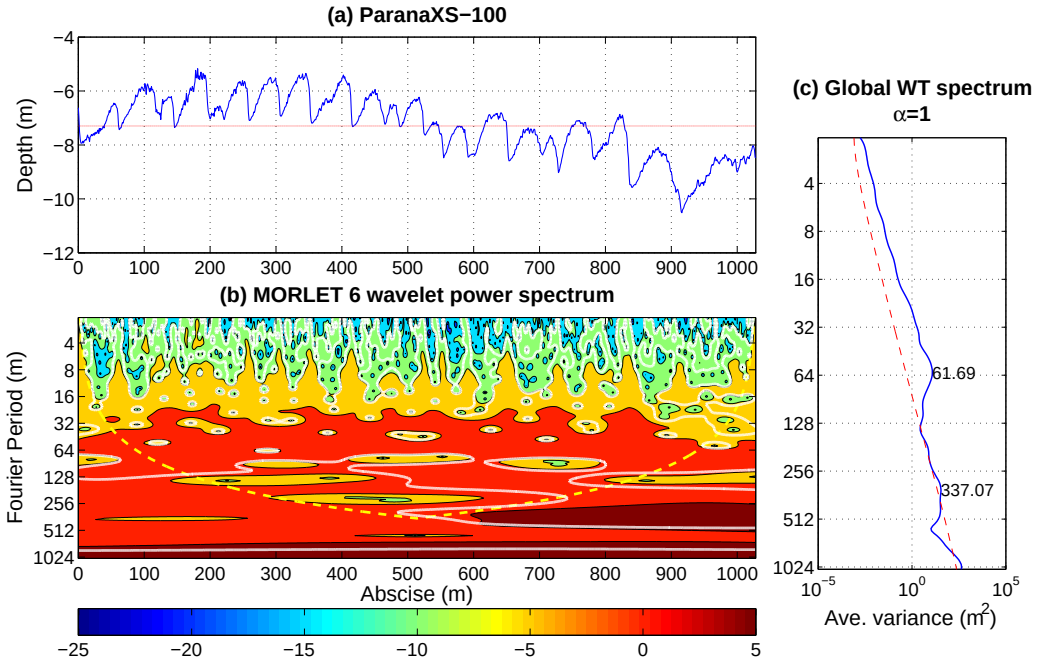

Figure 2.7: Wavelet analysis output for section j=100. Bedform migration from left to right. (a) Bedform profile at section j=100, (b) contours of the wavelet power spectrum using the Morlet WF, and (c) global wavelet power spectrum showing the main frequencies in section j=100. The higher frequency, 337 m, is used by the program to discriminate the third bedform hierarchy.

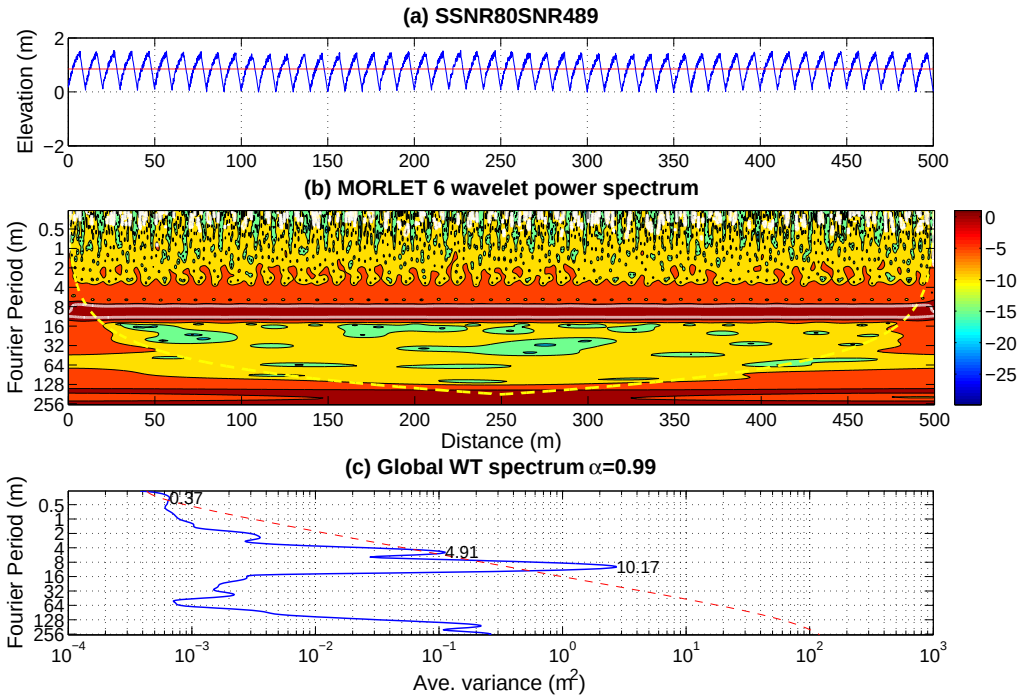

Figure 2.8: Wavelet analysis output for section synthetic signal SSNR80SNR489. Refer to to Figure 2.7.

for SSNR80SNR489 and j=100, respectively. These criteria are, as stated above, the objective criteria to define ripples and small dunes. The chosen signal then becomes the first level of the bedform discrimination ($\eta_{1,3}$ in Figure 2.9 and $h_{1,3}$ in Figure 2.10), and the corresponding $\hat{\eta}_2(s)$ and $\hat{h}_2(s)$ become the second level of the bedform separation ($\eta_{2,3}$ in Figure 2.9 and $h_{2,3}$ in Figure 2.10).

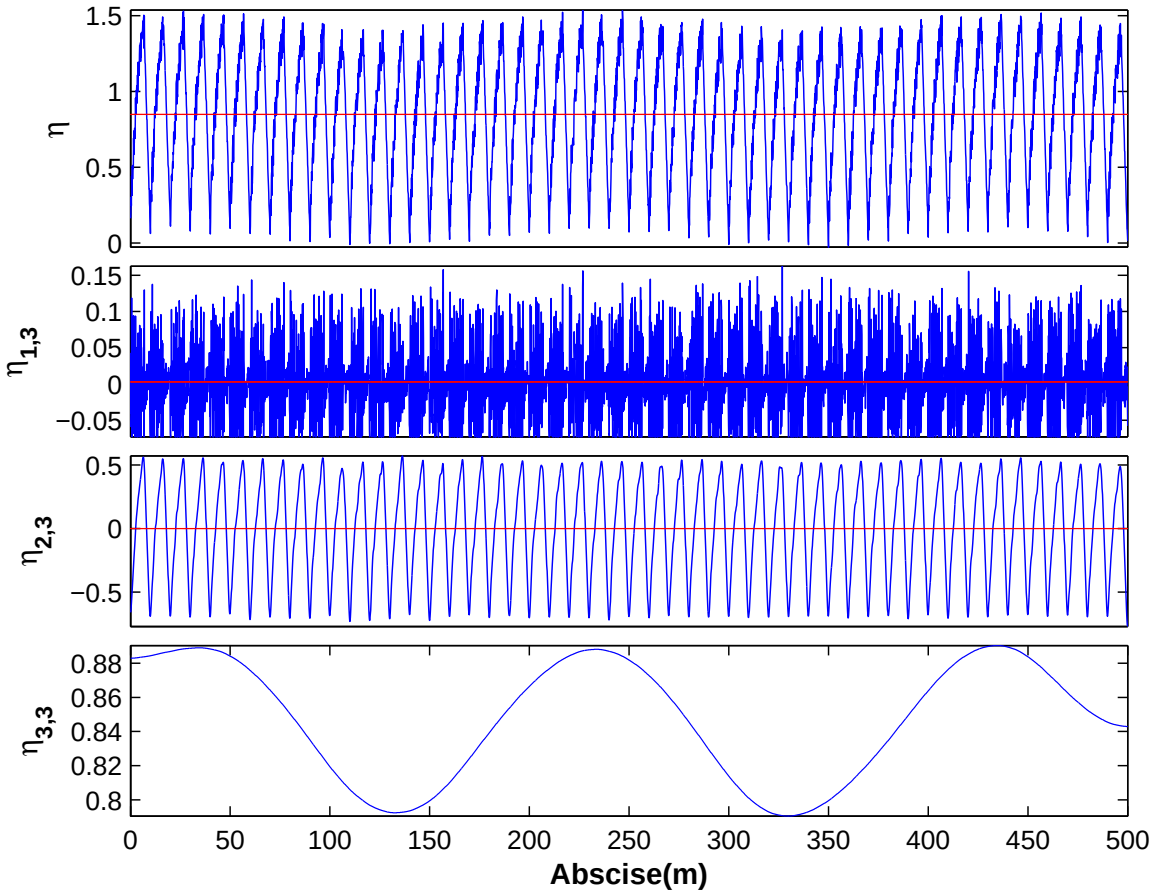

Figure 2.9: Wavelet analysis output for the synthetic signal SSNR80SNR489 (refer to Figure 2.10)

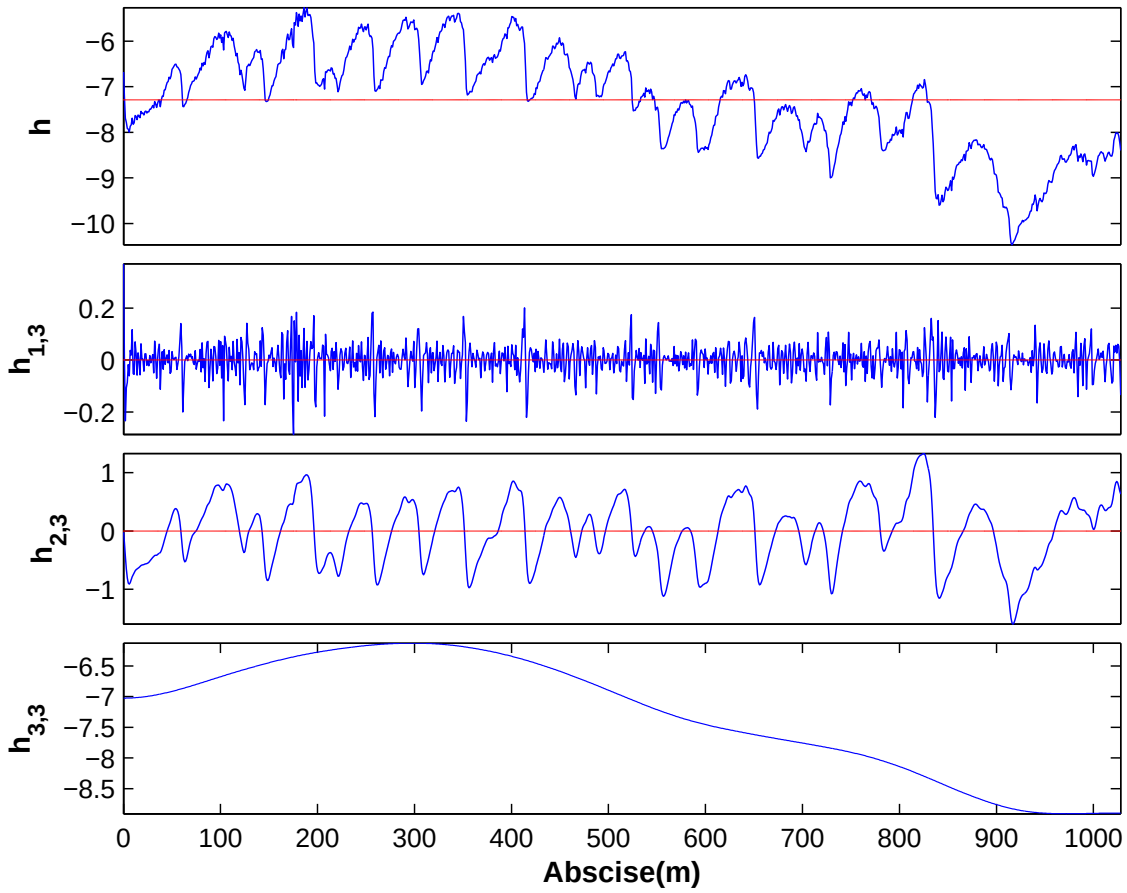

Figure 2.10: Wavelet-Spline discrimination output for section j=100. $h_{1,3}$ represents the first bedform hierarchy (small dunes), $h_{2,3}$ represents the second bedform hierarchy (large to medium size dunes), and $h_{3,3}$ represents the third bedform hierarchy (bars)

3.0 RESULTS

3.1 ACCURACY OF THE METHOD

The results reveal that the method presents high accuracy in retrieving information from the bars and dunes signals. A cross correlation analysis of the retrieved and actual bar and dunes signals is persistently higher than 0.9 at lags equal to zero for NR>50 at any SNR (see Figure 3.1b and Figure 3.1c), and Figures Figure 3.2b and Figure 3.2c). Likewise, their standard deviation ratios (see Figure 3.3b and Figure 3.3c) are markedly closer to one for NR>50 at any SNR. Filters, inexorably, induces some deformation on the filtered signals [67, 56]. This is particularly critical for retrieving ripple signals. A closer analysis of those signals indicates that the cross correlation between them are higher than 75% for NR>50 (see Figure 3.1a) and the robust spline filter does not lag the ripple signal as shown in Figure 3.2a. However, it distorts their amplitudes (see Figure 3.3a), especially for NR<50 and SNR<5. Most of the amplitude deformations take place in the troughs. It is important to note that among the different filters, the robust spline filter minimizes such trough or valley deformation [67]. The results reveal that this limitation of the filters is also improved when the points of the ripple signal with negative elevation, and below a 2.5 times the standard deviation threshold, are considered as outliers; and therefore, fixed at such threshold. The aforementioned quantities, reflect that improvement. In order to assess the reproducibility of the ripple frequencies, the reproducibility ratio, defined as the ratio between the number of common peaks (of the actual and retrieved ripple signals) detected in at least 50% of the whole spectra and the total number of peaks corresponded to the number of peaks detected across all the spectra [56],was quantified. In the present work, the wavelet spectra are used. The results point out that the reproducibility is higher than 70% for NR>50 (see Figure 3.4).

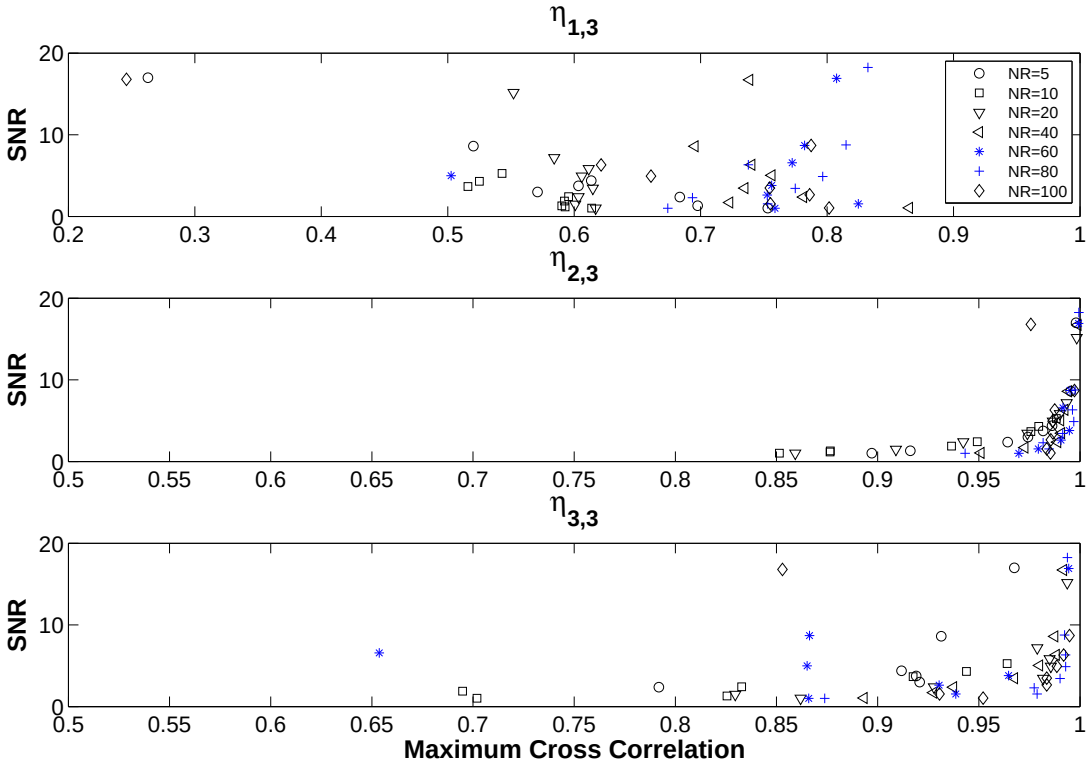

Figure 3.1: Maximum cross correlation between retrieved and actual (a) ripple, (b) dunes, and (c) bars synthetic signals

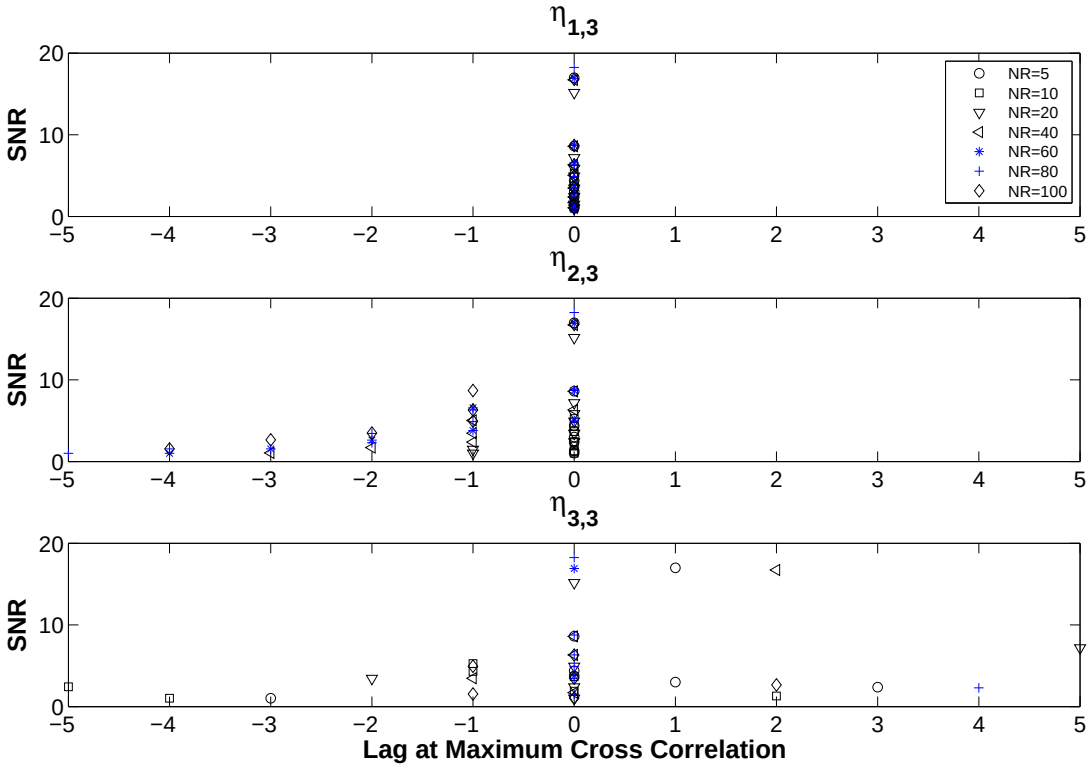

Figure 3.2: Lag at the maximum cross correlation between retrieved and actual (a) ripple, (b) dunes, and (c) bars synthetic signals

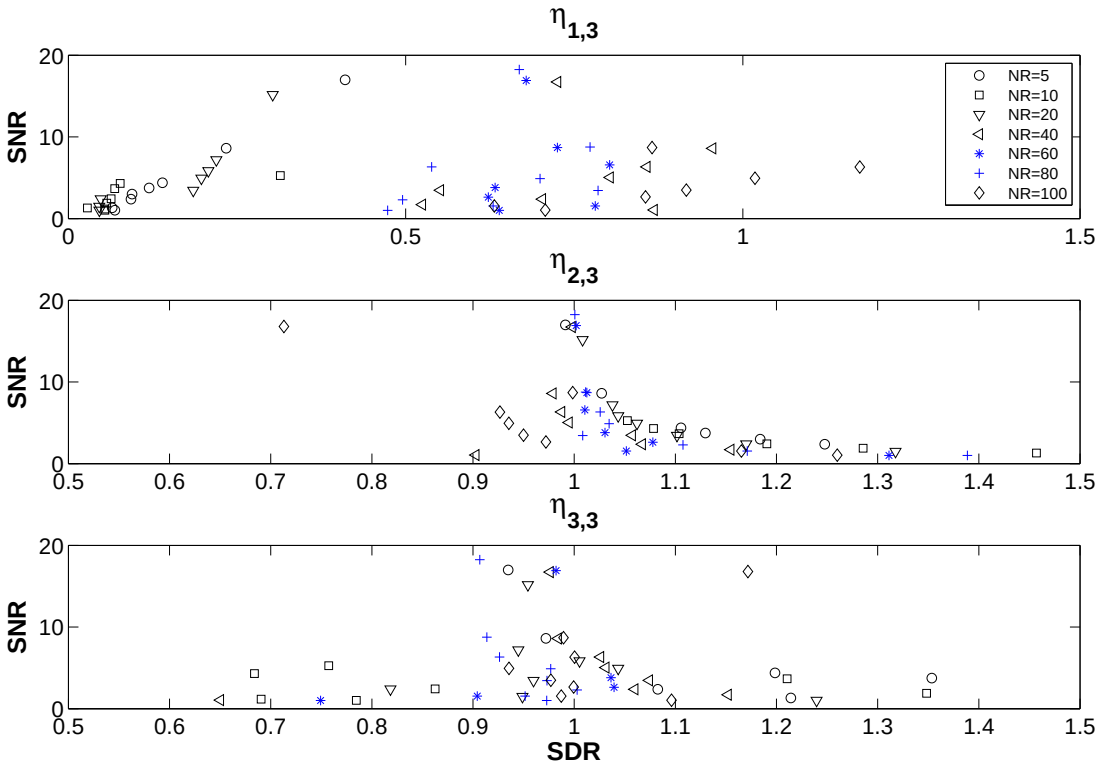

Figure 3.3: Standard deviation ratio between retrieved and actual (a) ripple, (b) dunes, and (c) bars synthetic signals

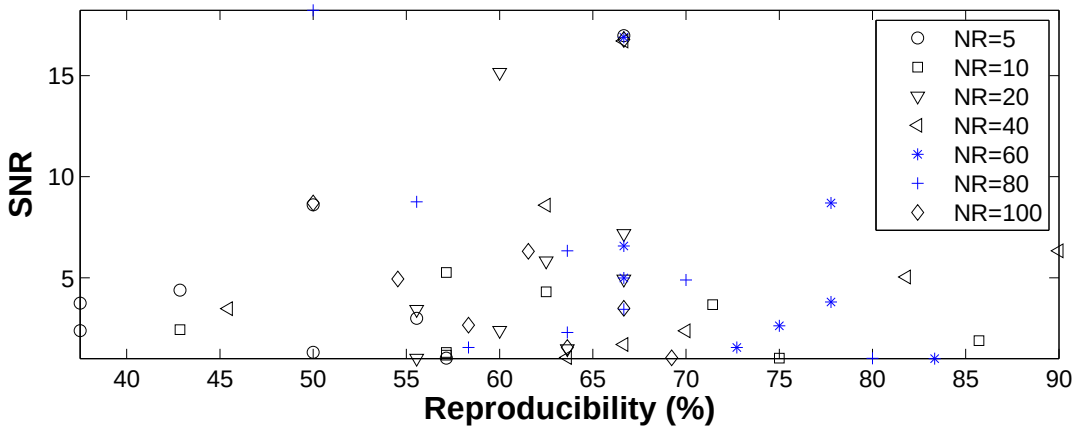

Figure 3.4: Proposed method reproducibility of the frequencies

3.2 DISCRIMINATION OF THE BEDFORM SCALES IN THE PARANA RIVER

After the aforementioned procedure is conducted on the 370 BFPs, various scales of bedforms are found and are presented in Figures 3.5, 3.6 and 3.7, respectively. Figure 3.5b shows that for the case of markedly 3D medium and large dunes, the small dunes with higher amplitudes are concentrated near to the troughs and that their amplitudes tend to increase as they approximate to the peaks, denoting that the process of forms amalgamation is prevalent in 3D dunes. This pattern is not recurrent for large dunes that subparallel with their neighbors and is explained by the fact that obliquity of the crest influences the length of any separation zone and thus influences the magnitudes of the leeside Reynods stresses, drag coefficients and the dispersal patterns of sediments .Figure 3.6 shows that crestal platforms are commonly present is markedly 3D shallower large dunes. According to Maddux et al. [53],the turbulence generated by 3D dunes is weaker than the 2D case, due to the generation of secondary flows over the 3D forms. Thus, in shallower areas there is a massive creation of dunes, instead they are eroded. Figure 3.7 shows that the bar is highly variable along the morphology survey. Therefore, a linear representation of it had been too simplistic.

The wavelet analysis using the Morlet WT (Eq. 2.11) on the $\hat{h}_3$ signals was also conducted, and the average wavelet power spectrum, namely power Hovmöller, for 4-8 m and 8-16 m bands was obtained. The power Hovmöller is a 2D contour plot used to display the wavelet variance of the bedform profile along the x-axis at distinct transverse locations, y. This 2D contour plot allows assessment of the variability of the power distribution in both the longitudinal and transverse directions, as well as isolation of features characterized by a certain range of dimensions, such as wavelength [17]. The contours are plotted for the entire survey area that is represented in a grey scale. Figure 3.8a indicates that the higher frequencies are located mainly in the troughs and at the crest of some dunes. Likewise, Figure 3.8b indicates that the second band is densely distributed in the dunes surveyed, especially close to the troughs.

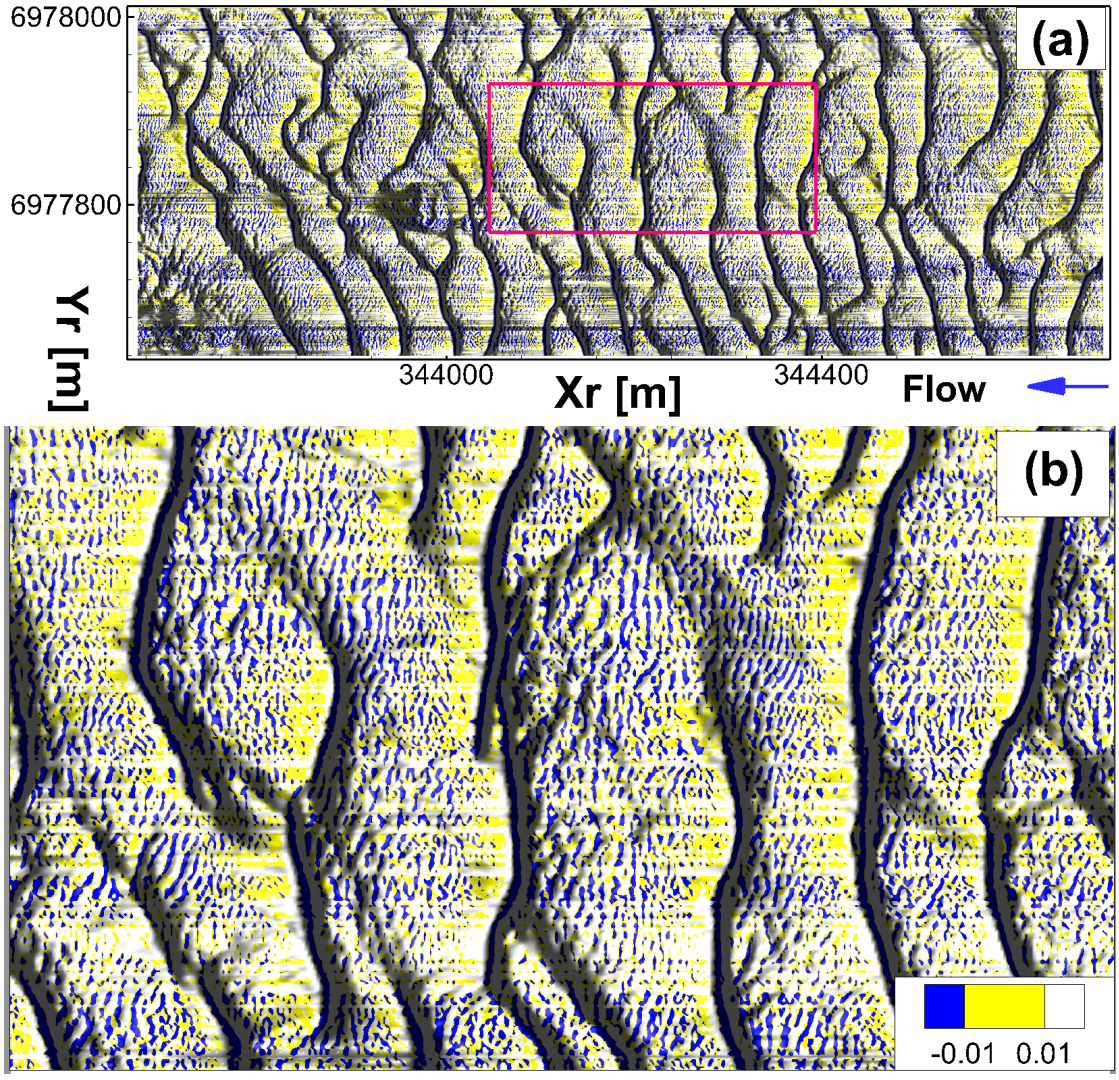

Figure 3.5: (a) $h_{1,3}$ (small dunes) data of the Paraná River survey, and (b) inset of small dunes superimposed to markedly three-dimensional larger dunes. Recurrently, in this case the smaller dunes (yellow areas) concentrate at the bottom and grow in amplitude as they get closer to the peaks. Flow is from right to left

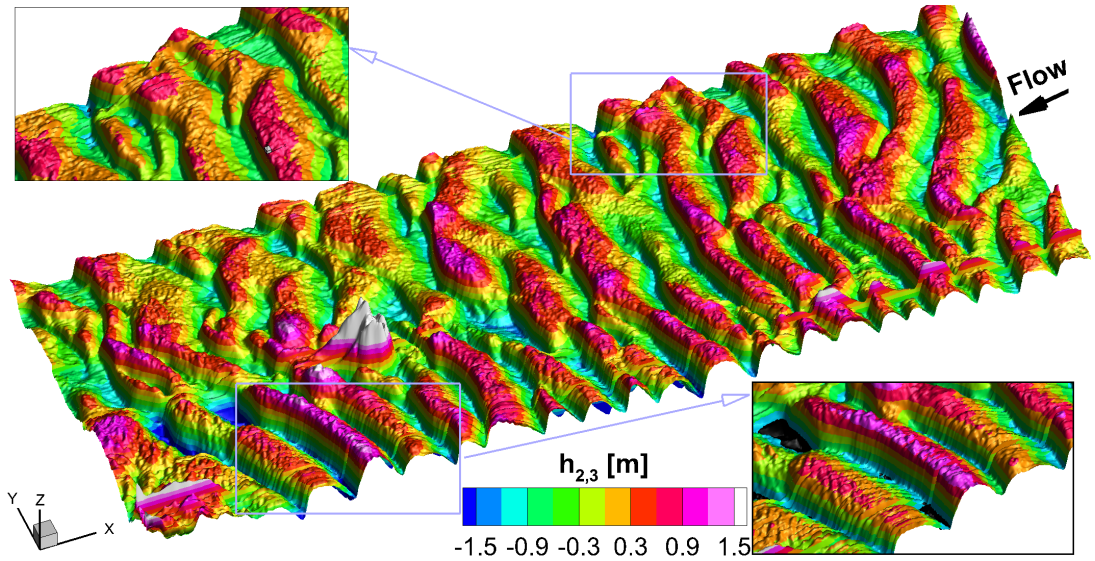

Figure 3.6: $h_{2,3}$ (medium to large size dunes) data of the Paraná River swath. Note that crestal platforms are developed at shallower markedly three-dimensional larger dunes. Sub-parallel larger dunes tend to be more two-dimensional. Bedforms migration from right to left.

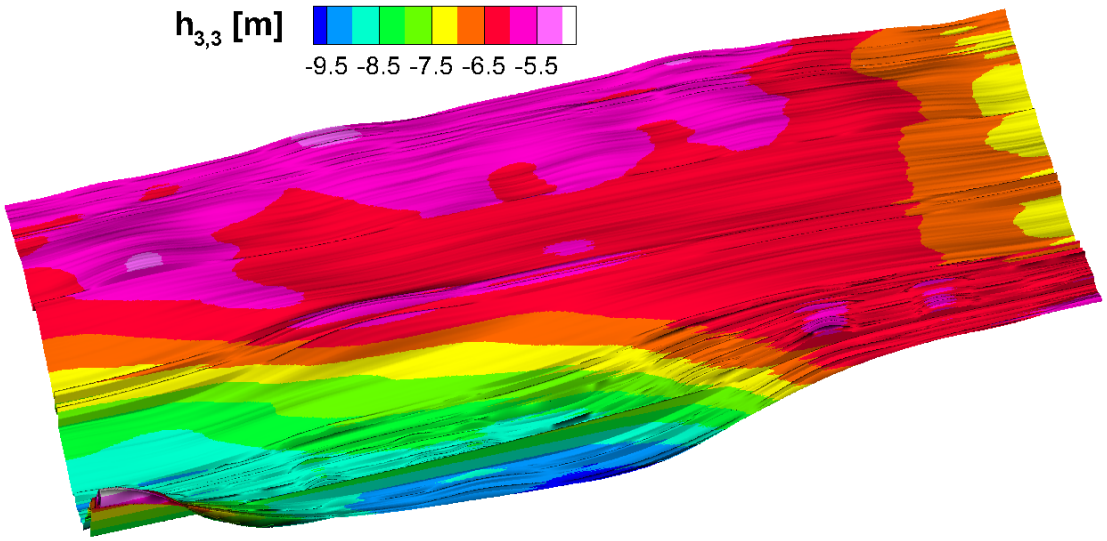

Figure 3.7: $h_{3,3}$ (bars) data of the Paraná River survey. Flow is from right to left. This bedform hierarchy imposes a highly non-stationary condition on the BFPs. A linear representation of it would be too simplistic for this survey.

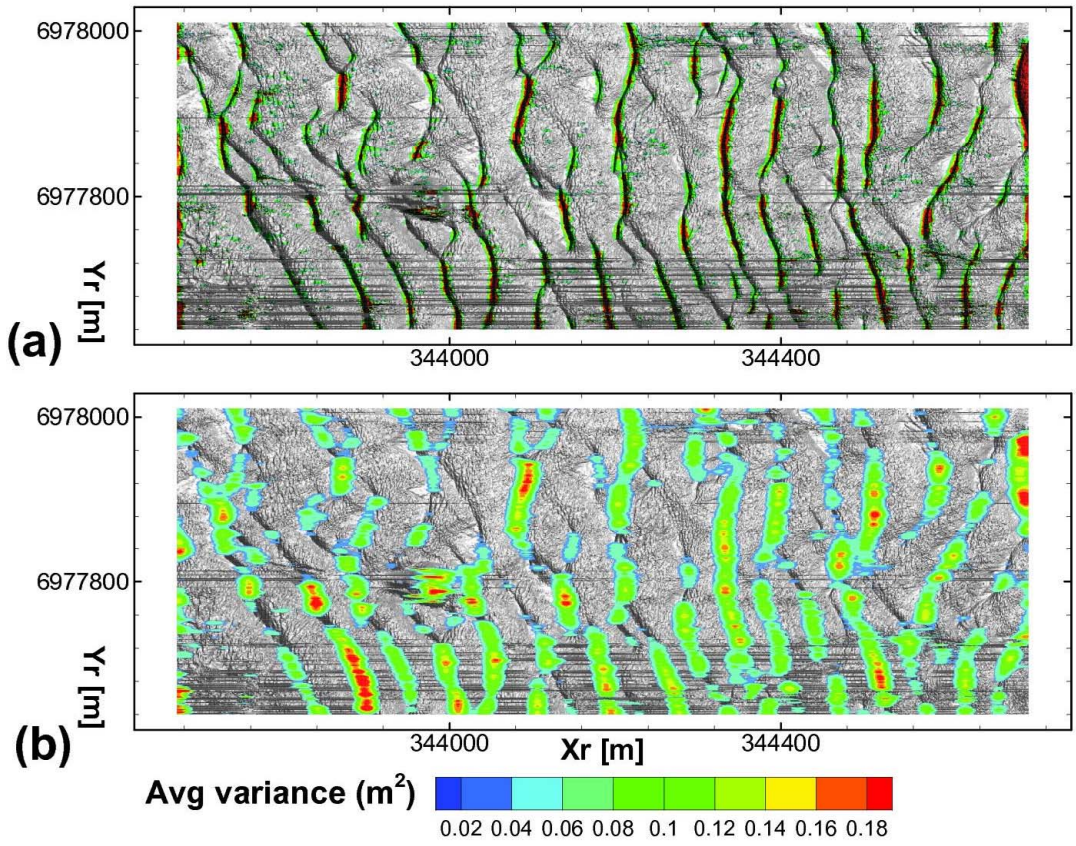

Figure 3.8: Power Hovmöller of the averaged wavelet power spectrum for two scale bands of the $h_{2,3}$ swath: (a) $[4-8]$m (small dunes), (b) $[8-16]$m (medium size dunes). In all cases the contours present the variance with a 95% confidence level.

3.3 THE STATISTICS OF BEDFORM FEATURES

The data for different size dunes, filtered as the signal of the smallest bedforms over the stoss side of the larger dunes are analyzed statistically later. The histograms of the dune descriptors (see Figure 3.9) show that there is a marked dierence in the distribution of the wavelength of smaller features on the lee and stoss sides. Similar results were reported by [33, 24, 44, 45] .

Figure 3.10 demonstrates that there is correlation between the wavelength and the amplitude of these superimposed smaller features for the stoss side, but not the lee side.

The probability distribution functions (PDFs) of the dimensionless descriptors of the large and small dunes are shown, with the Weibull, Gaussian, Gamma, GEV, and Pareto distributions in Figures 3.11-3.14. In each case, a dimensionless value of each descriptor is defined as the descriptor divided by its mean value. The goodness of fit of some distribution functions was evaluated by the Anderson-Darling test (denoted A2; see Table 3.1) that allows the testing of a wider range of distributions where some of the parameters may not be known [19].The minimum A2 denotes the best PDF.

As shown by in Figures 3.11-3.14 and 3.1, in most of the cases the Gamma distribution provides the best goodness of fit. Likewise, all the parameters show a positive skewness and leptokurtic distribution.

A similar analysis was performed on the small dune sample population (see Figures 3.9 - 3.17 and Table 3.1). The histogram (Fig. 3.15) demonstrates that the wavelength of these bedforms on both the stoss and lee sides present the characteristics of discrete variables. On the other hand, the absolute value of their amplitudes reveals that the characteristic amplitude is approximately 0.05 m. The slopes, when compared to that that of the dunes, presents lower values in the stoss side and similar values in the lee side. The Gamma distribution presents the best goodness of fit, with the kurtosis being positive, greater than that of the larger dunes, and with a leptokurtic distribution.

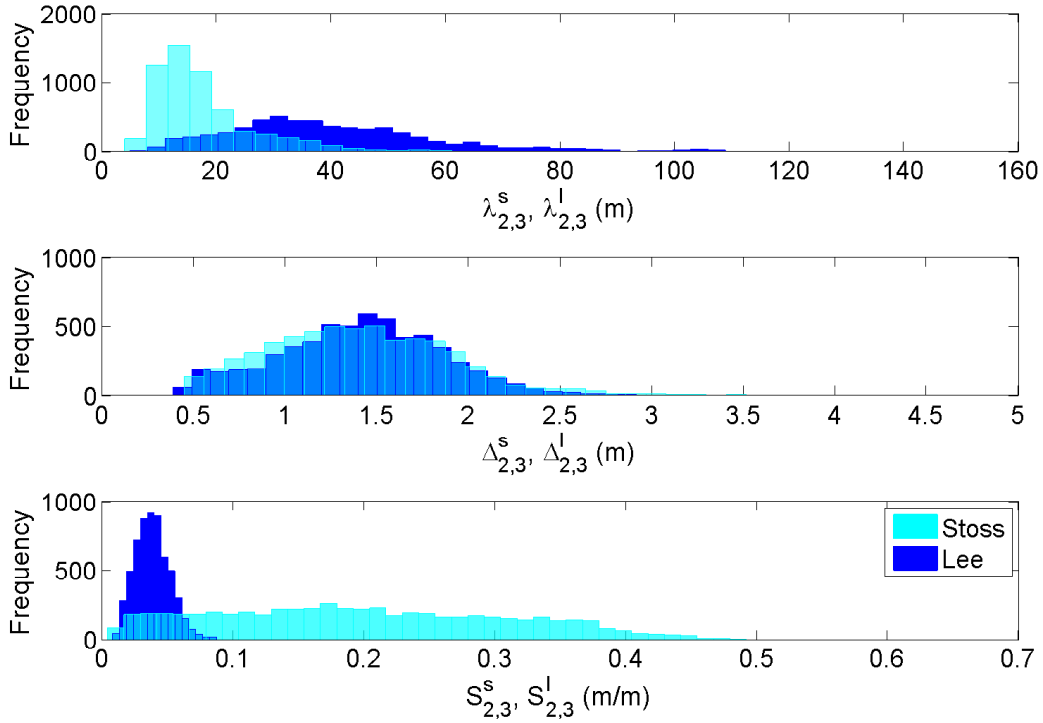

Figure 3.9: Histograms of the dune descriptors. The wavelength at the stoss side ($\lambda^l_{2,3}$) shows higher variability than that of the stoss side. The amplitudes at the stoss and lee sides ($\Delta^s_{2,3}$ and $\Delta^l_{2,3}$) show similar distribution of frequencies. The slope at stoss side ($S^s_{2,3}$), that is closely related to the angle of repose of the sediment material, shows an almost even distribution: however, the slope at the lee side ($S^l_{2,3}$) shows higher variability.

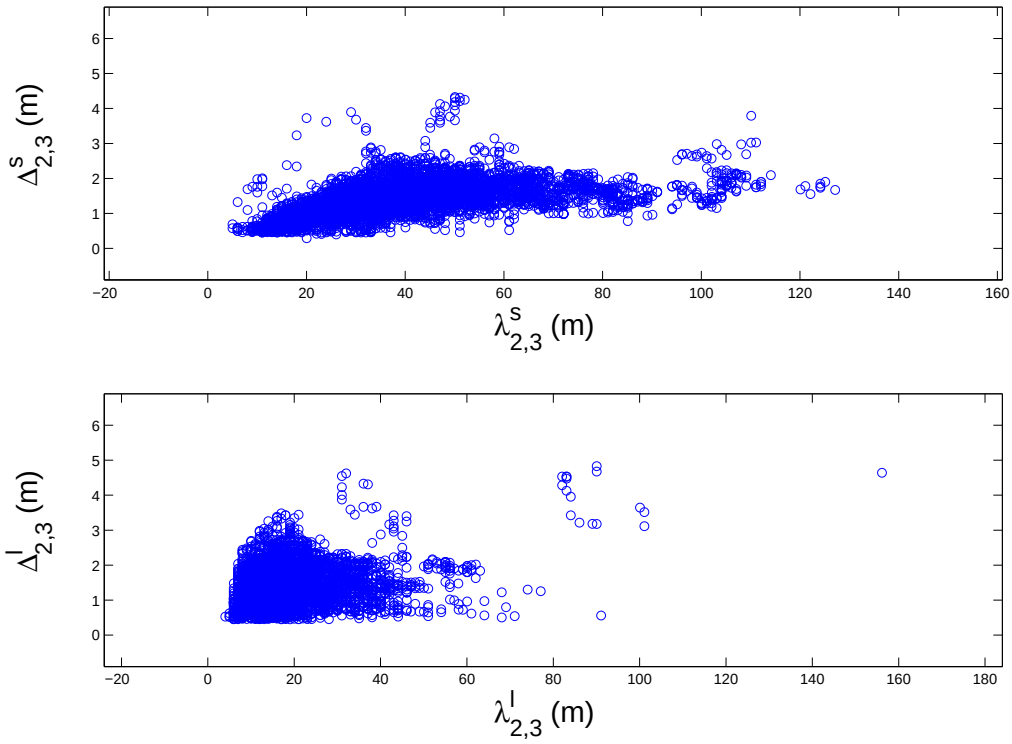

Figure 3.10: Dune stoss and lee scatter plots. Note the strong correlation between the wavelength and amplitude of the dune stoss and lee sides. Not such correlation is present in the lee side

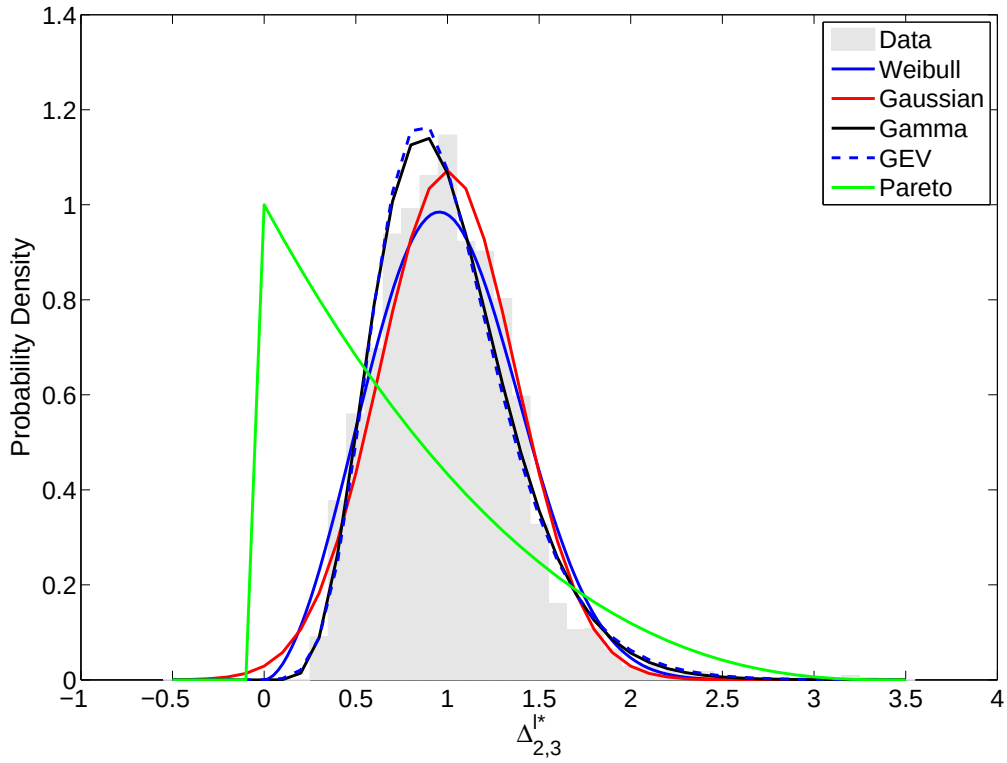

Figure 3.11: Probability distribution of the dimensionless larger dunes lee amplitude.

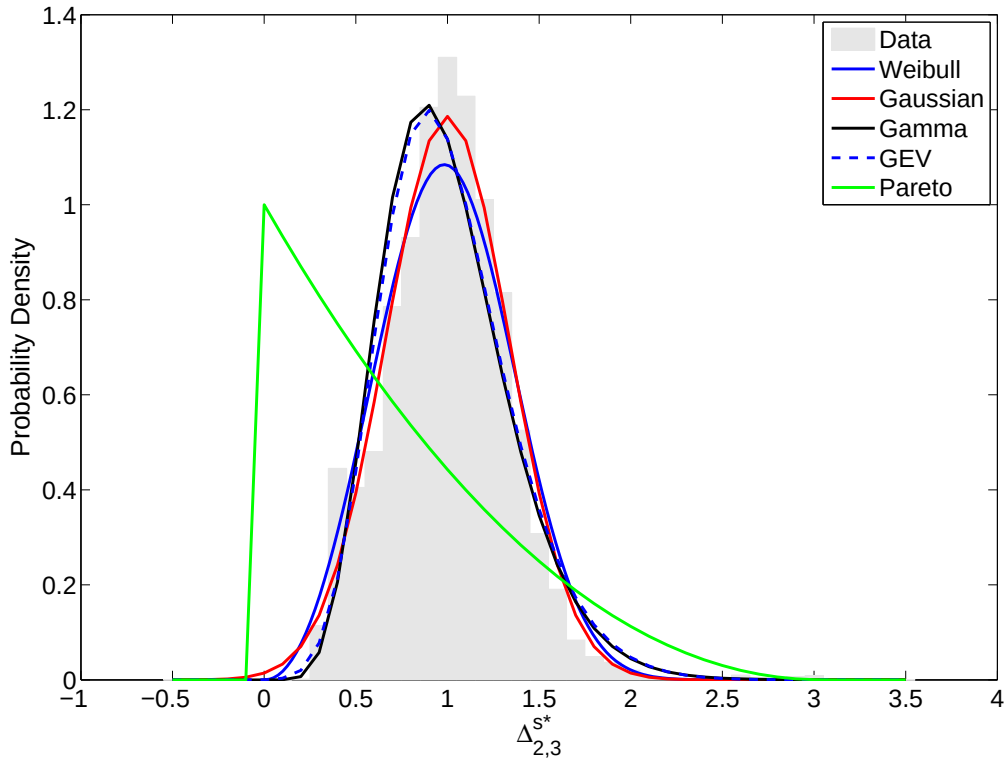

Figure 3.12: Probability distribution of the dimensionless larger dunes stoss amplitude

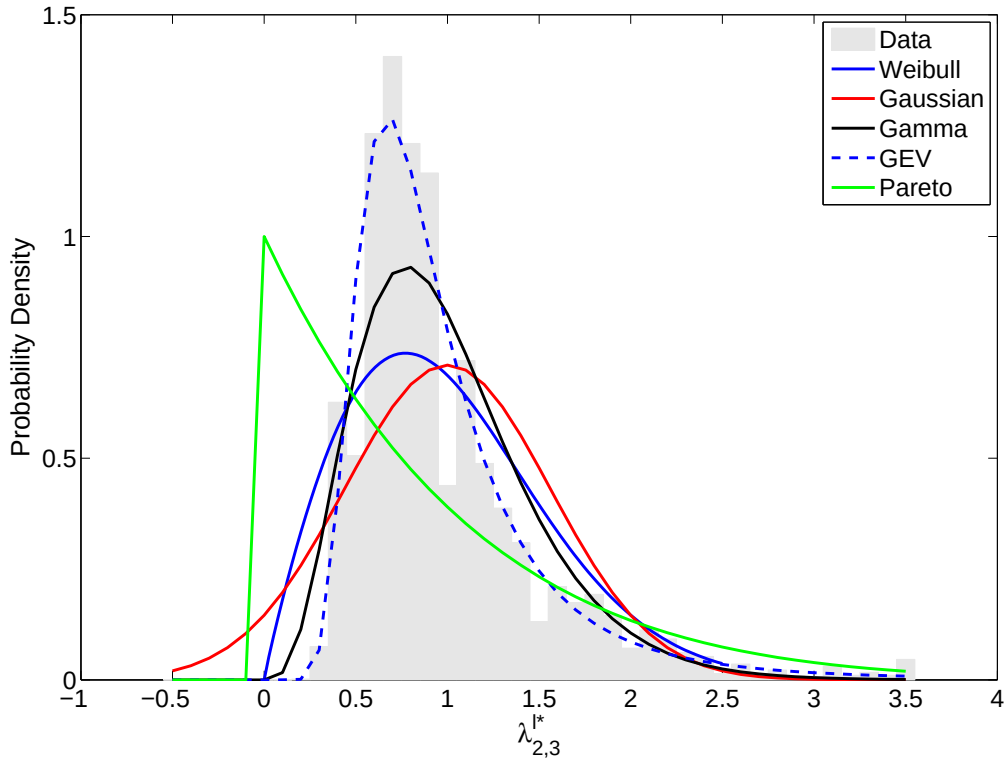

Figure 3.13: Probability distribution of the dimensionless larger dunes lee wavelength

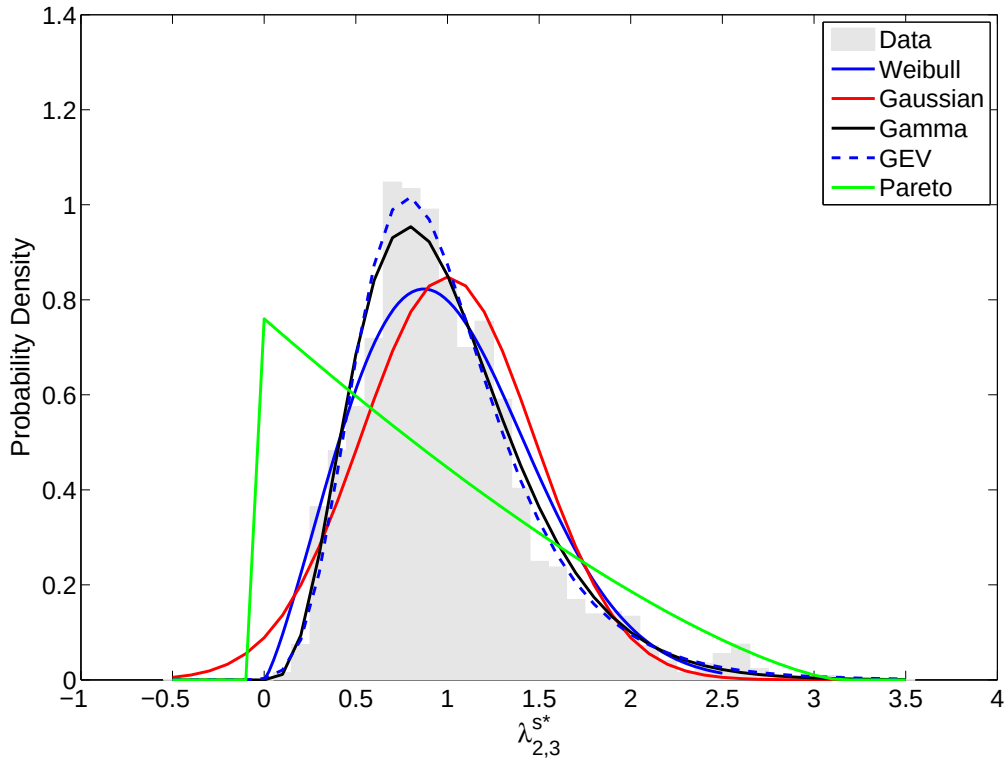

Figure 3.14: Probability distribution of the dimensionless larger dunes stoss wavelength

Table 3.1: Anderson-Darling test results

Descriptor	Gaussian	Weibull	Gamma	LEV
$\Delta^l_{1,3}$	1223.694	142.025	24.039	125.096
$\lambda^l_{1,3}$	3051.354	2760.217	3117.411	3521.328
$S^l_{1,3}$	2075.473	300.636	221.084	707.954
$\Delta^s_{1,3}$	2131.653	158.549	46.618	282.053
$\lambda^s_{1,3}$	9282.491	8610.33	9927.283	11561.65
$S^s_{1,3}$	3327.436	340.417	114.906	622.001
$\Delta^l_{2,3}$	22.591	27.246	9.063	20.916
$\lambda^l_{2,3}$	271.859	173.389	80.168	56.153
$S^l_{2,3}$	35.957	35.233	65.794	40.963
$\Delta^s_{2,3}$	9.208	25.055	38.174	65.365
$\lambda^s_{2,3}$	83.835	41.148	6.286	3.578
$S^s_{2,3}$	46.79	82.481	5.844	14.675

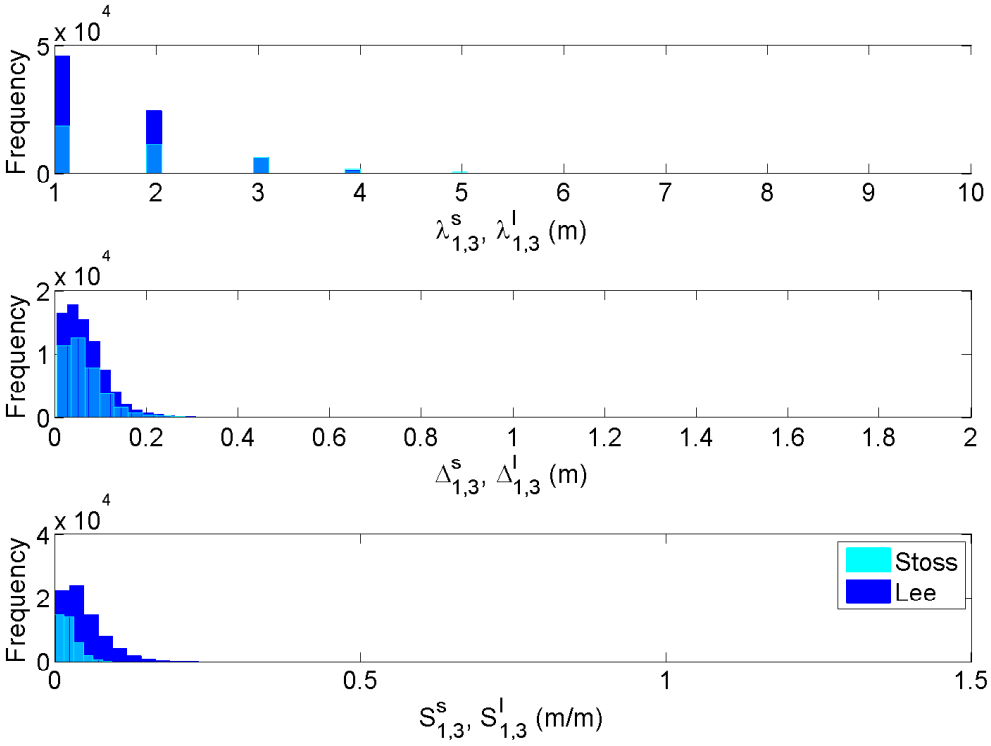

Figure 3.15: Histograms of the small dunes descriptors. Note that the wavelengths at the stoss and lee sides ($\lambda^s_{2,3}$ and $\lambda^l_{2,3}$) the continuity of the interval is strongly determined by the sampling frequency. The amplitudes at the stoss and lee sides ($\Delta^s_{2,3}$ and $\Delta^l_{2,3}$) shows similar distribution and since small dunes represent shorter life-span structures, they appear to be related to the angle of repose of the sediment material any more.

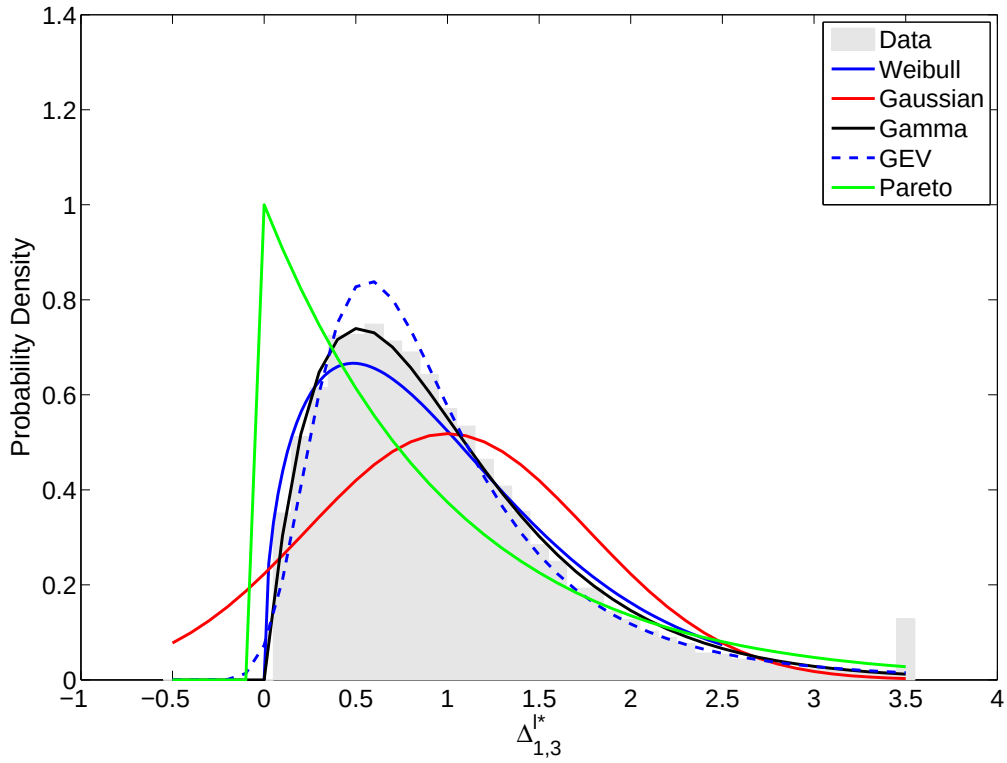

Figure 3.16: Probability distribution of the dimensionless small dunes lee amplitude

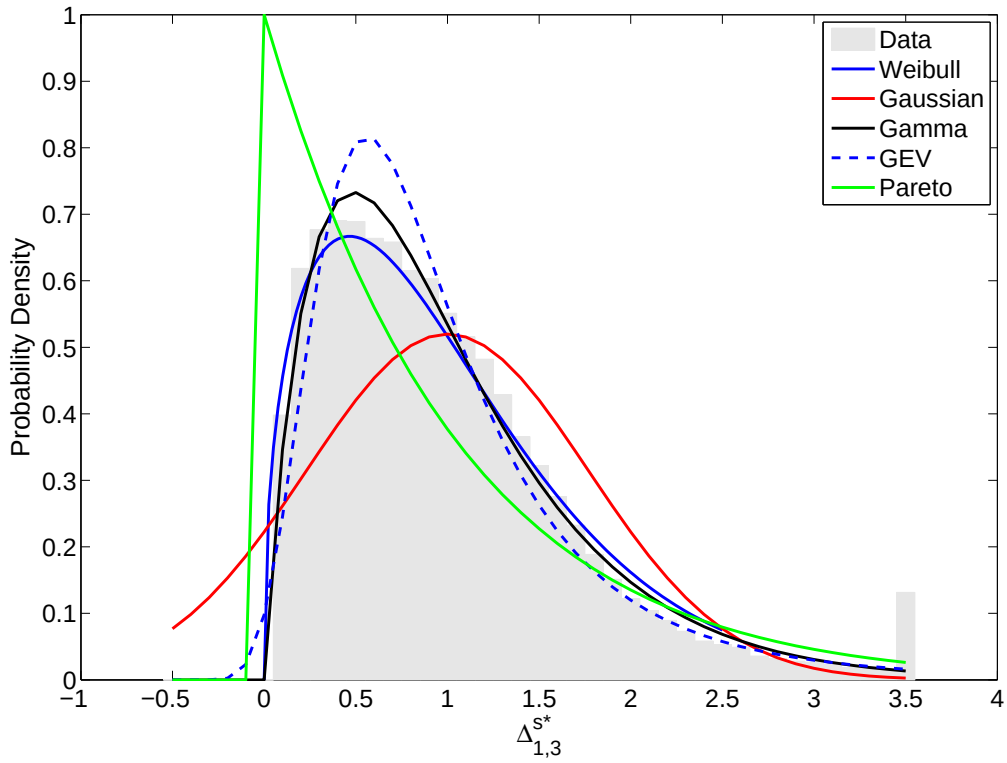

Figure 3.17: Probability distribution of the dimensionless small dunes stoss amplitude

4.0 DISCUSSION

4.1 DISCRIMINATION METHOD

The proposed method is based on the scaling definition of dunes and ripples, it is applicable to laboratory and field measurements and overcomes the limitations of using a moving average and spectral analysis. The program allows the user to define the third level based on his/her scales of interest.

In the present contribution, it is successfully used in discriminating larger bars and different scales of dunes. By analyzing synthetic signals, the procedure has shown to perform well in retrieving and quantifying the various scales of waves within a bedform series (up to the third level wave) when at least one period of such a wave is present in the BFP, as shown in Figures 4.1 and 4.2, although it does impose some waviness where no single period is present (see Figure 4.3). This limitation dramatically distort the characteristics of the dunes. The program solves for the s parameter that minimizes this limitation. Thus, the retrieved bar signal is still more suitable than using a linear trend line that may not be applicable for large rivers such as the Paraná River, where the mean river bed is fluctuating, rather than linear [77].

Some researchers ([77, 24]) point out that the definition of ripples as entities that have lengths less than 0.60 m is restrictive. Other researchers (e.g. [50]) successfully used such threshold. Coleman and Nikora, 2011 ([18]) suggests the use of a threshold bedform height to distinguish transient sand pile ups from stable bedforms resisting flow. The estimates demonstrates that even though the ripple definition is limited, when coupled with the capabilities of both robust spline filter and wavelet transforms such widely accepted discrimination criterion can retrieve relevant information of both ripples and dunes for their lee and stoss

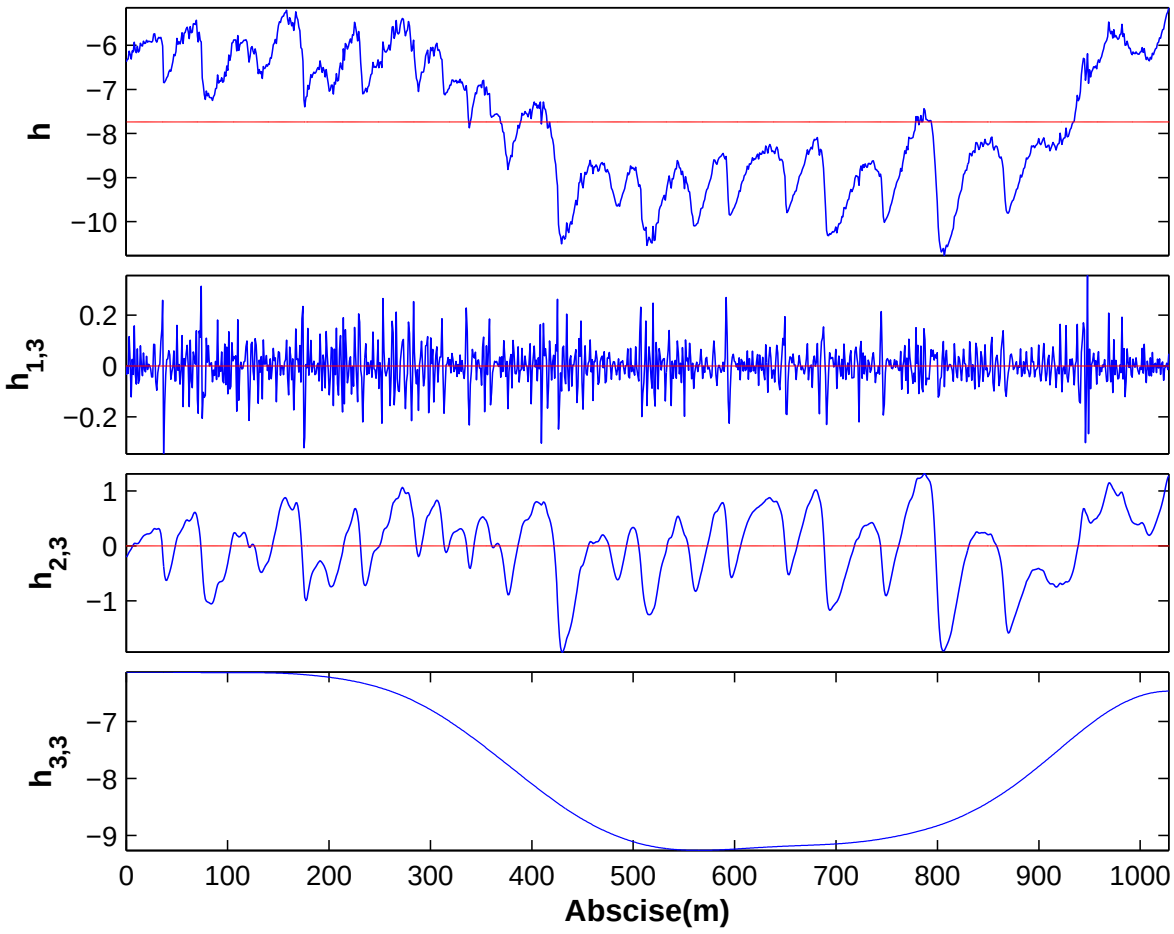

Figure 4.1: Discrimination of different bedform scales output for transect j=20. Flow is from left to right

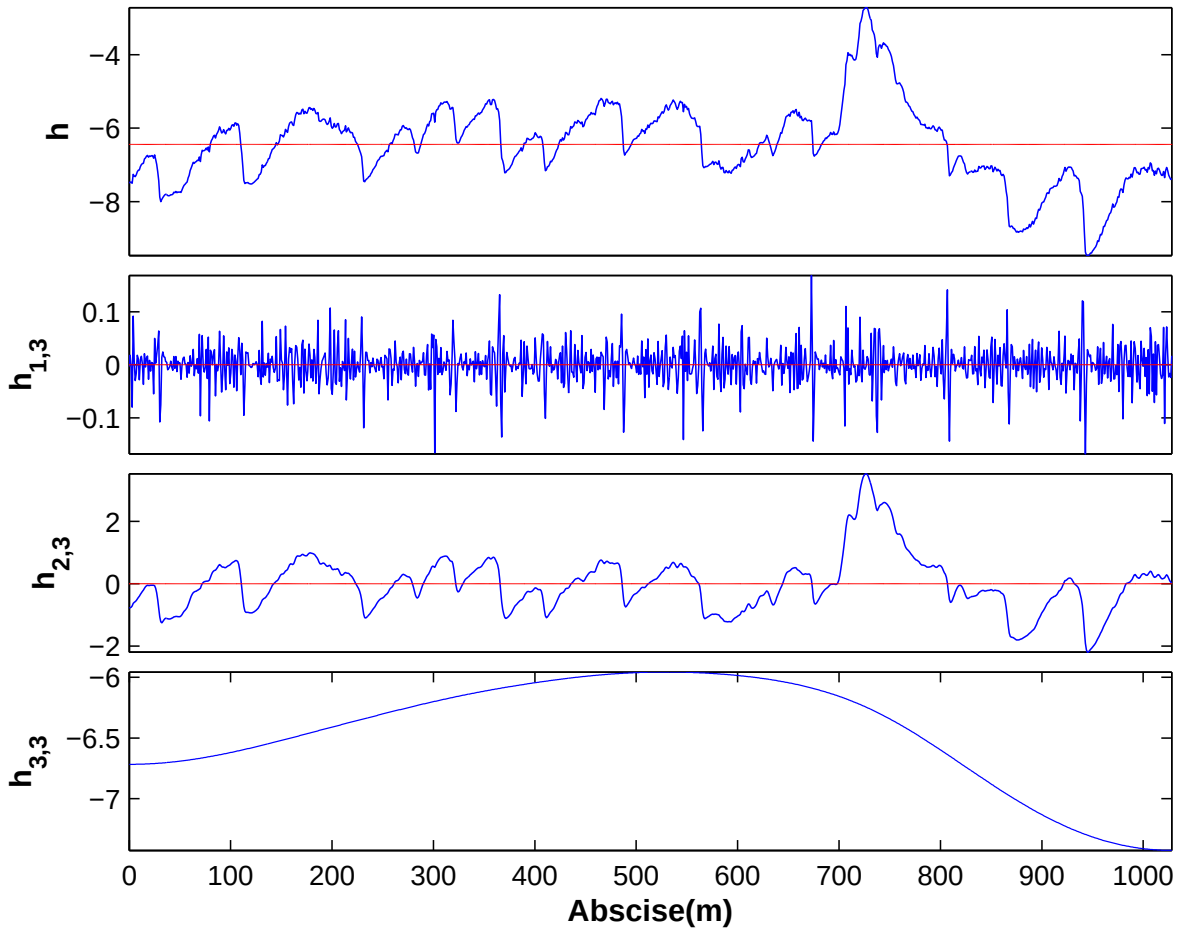

Figure 4.2: Discrimination of different bedform scales for transect j=161. Flow is from left to right

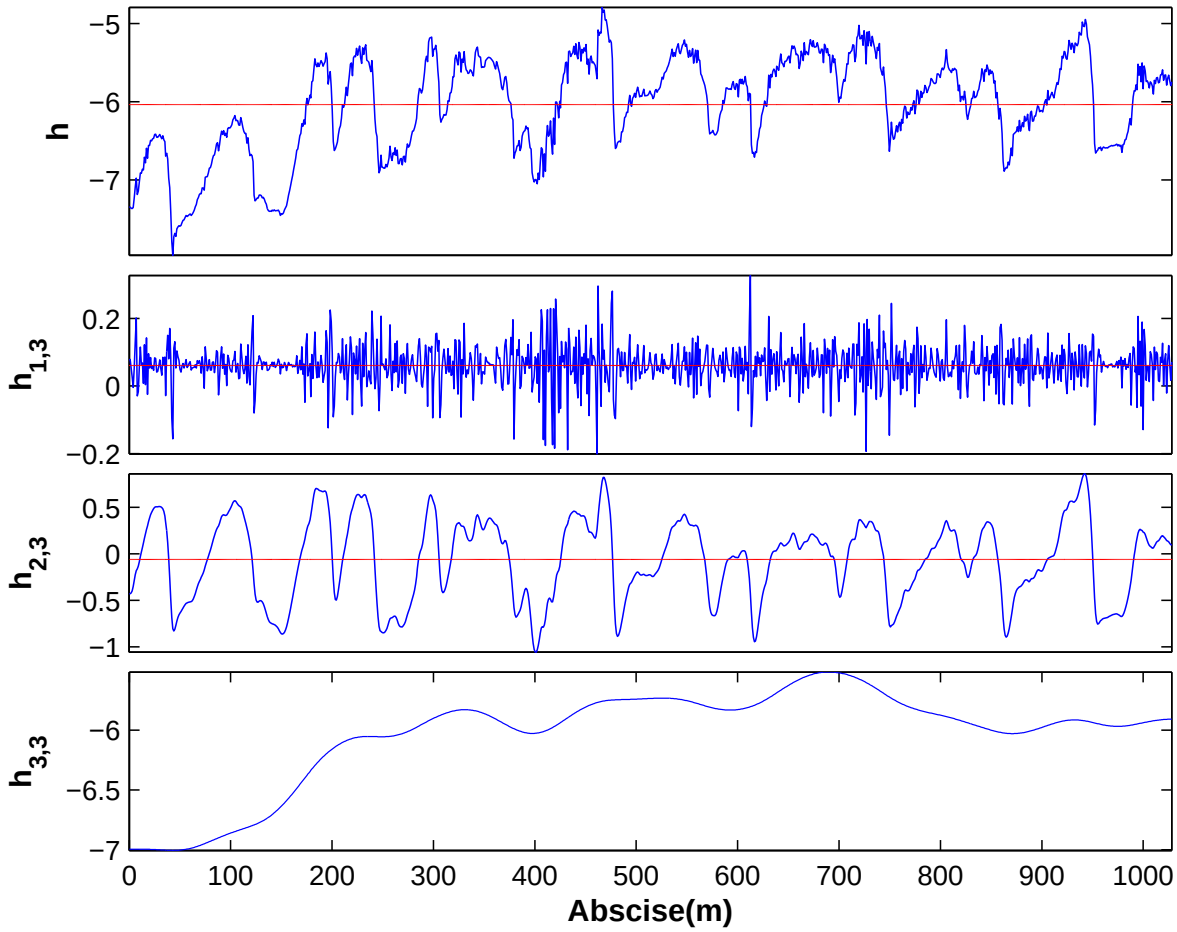

Figure 4.3: Discrimination of different bedform scales output for transect j=350. Flow is from left to right

sides. Unfortunately, no many studies have focused on the transitional areas between bedform states, even though they are critical to explain bedform scales, apparently such studies have attracted far less attention than studies of bed forms in the middle of their stability fields ([9, 13, 10]).

I believe that when the understanding of the ripples is improved, a dynamic threshold will be applied. Up to date, the aforementioned ripple definition represents the ocial criterion to distinguishing between ripples and dunes [37], although it is based on an observational gap. However, if in certain cases ripples are over or under represented by such threshold, our proposed method can still retrieve the ripple signal with a reasonable level of accuracy as demonstrated by the results of the synthetic signals analysis.

By using wavelet transforms, the distribution of the wavelengths of small dunes can be estimated, and by using the robust spline filter the distribution of the amplitude of bedforms within the Paraná River can be analyzed.

4.2 THE STATISTICS OF BEDFORMS

The bed morphology of the Rio Paraná comprises bars (unit, point, complex bars), dunes and ripples with three-dimensional characteristics [65]. Bars have wavelengths from 325 m to >450 m, and generally larger bars are associated with larger dunes. A similar trend has been reported by [46] who studied the possible interaction between dunes and bars, and showed that the nonlinear coupling between relatively short (dunes) and long (bars) wavelength forms may cause the growth of the bars.

The dunes within the present reach are markedly asymmetric with the lee slope being nearly four times that of the stoss slope. In many instances in the present analysis, the dune signals show that a higher trough-scour depths, relative to mean bed level, are succeeded by a higher upstream dune. As shown in Figure 2.3 the small dunes exhibit irregular three-dimensional features. These entities are similar to linguoid ripples which form under higher bed shear stresses and represent the second stage of the transition from ripples to dunes as reported by [68].

If similarly to the signal to noise ratio, the dune-to-ripple ratio (DRR) is set as the ratio of the standard deviation of $\hat{h}_3$ and that of the small dunes, the results show that the DRR is highly variable and is not correlated with the average water depth (see Figure 4.4a). This was expected since some of the descriptors of the ripples are governed by the sediment size (and other parameters), but essentially are independent of the water depth [21]. Likewise, Figure 4.4b demonstrates that the standard deviation of the ripples presents a relative high redundancy when compared with that of $\hat{h}_3$.

The Anderson-Darling test was applied to estimate the goodness of fit of the PDFs, which in past studies has been assessed using a relative error [78] and the Kolmogorov-Smirnov Test [80]. However, the Kolmogorov-Smirnov test presents two main limitations: [1] it tends to be more sensitive near the center of the distribution than at the tails and, [2] perhaps its most serious limitation is that the distribution must be fully specified. Importantly, if the location, scale, and shape parameters are estimated from the data, then the critical region of the K-S test is no longer valid, and typically must be determined by simulation [59]. Use of the Anderson-Darling test as proposed herein, overcomes these limitations and appears a more useful technique as a standard basis.

The PDFs of the dimensionless descriptors of bedform characteristics vary for dierent hierarchies. The PDF that best describes the dune descriptors is the Gamma and Weibull functions, whereas the smaller dunes are best represented by the Gamma distribution. In all cases, the PDFs possess a positive skewness and leptokurtic distributions. Results from past studies show dierent PDFs for these descriptors. Some researchers found that the wavelengths, amplitudes and heights are best described by an exponential probability law [5]; bedform height by Rayleigh, Weibull, Gamma, Gaussian, and Beta distributions [78]; for bedform height and wavelength the Gaussian, Gamma and Weibull distributions, and the Weibull distribution was best for distributions of crest elevation, trough elevation and lee face slope [78]. Apparently, the PDFs of the bedform descriptors are very sensitive to the preprocessing procedure. The lack of a standard denition of their scope also triggers dierent results. Because of this fact, it is not reasonable to compare these results with those of past studies.

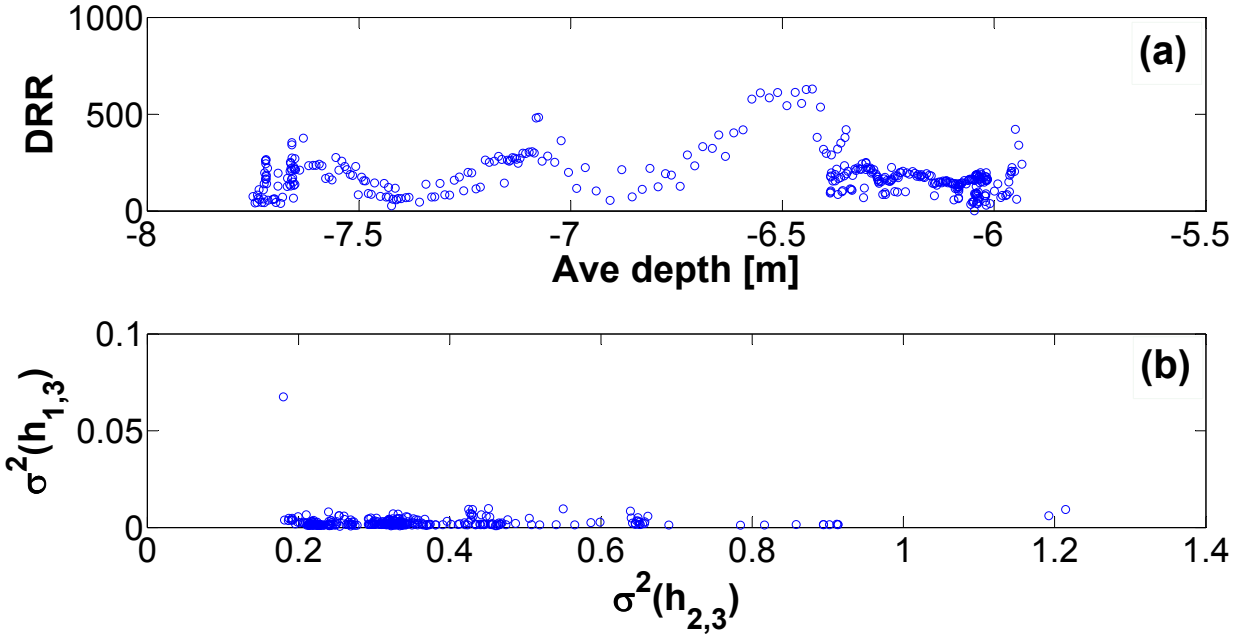

Figure 4.4: (a) DNR vs. transect average water depth. (b) $\sigma^2(h_{1,3})$ vs. $\sigma^2(\hat{h}_3)$

5.0 CONCLUSIONS

The synthetic bedforms comprised wavelength scales ranges up to four orders of magnitude (bars of 200m and ripples of 0.1m) for the case of NR=100. For such spectrum of frequencies the proposed method effectively retrieve information of bars and dunes with a high accuracy for NR>50 and SNR closer to 5. For the case of ripples, it retrieves a signal that is 75% correlated with the actual signal for NR>50. Likewise, it retrieves around 70% of the wavelengths and 70% of the actual ripple amplitudes when the NR is higher than 50 but slightly decreases as the NR is increased. In cases where the frequency range is higher, the accuracy will tend to decrease as explained by the Heisenbergs uncertainty principle.

The discrimination of different scale bedforms is important in order to study the geometric variability of bedforms, and quantify the influence of bedforms on the flow field and flow resistance. The present thesis has developed a methodology that combines the capabilities of continuous wavelet transforms and a robust spline filter to discriminate waves with dierent periodicities in bedform profiles, and applied this methodology to the 3-D bedform data from the Rio Parana, Argentina.

This thesis proposes a symbolic representation of bedform descriptors (e.g. wavelength, amplitude and slope) for each hierarchy (e.g. small dunes, dunes, bars) and the delimitation of such descriptors that is in line with past model, laboratory and field studies. The procedure has successfully retrieved the descriptors of the dunes and ripples hierarchies for both the stoss and lee sides.

Since bedforms in natural channels are predominantly three-dimensional in planform, foresee such two-dimensional wavelet transforms, when coupled with two-dimensional robust spline filters, would substantially improve the discrimination methodology proposed in this thesis.

BIBLIOGRAPHY

[1] J Aberle, V. Nikora, M. Henning, B. Ettmer, and B Hentschel. Statistical characterization of bed roughness due to bed forms: a field study in the Elbe River at Aken, Germany. *Water Resources Research*, 46, 2010. doi:10.1029/2008WR007406.

[2] Paul Addisson. *The illustrated wavelet transform handbook*. Institute of Physics Publishing Bristol and Philadelphia, United Kingdom, 2004.

[3] J. R. L. Allen and P. F. Friend. Relaxation time of dunes in decelerating aqueous flows. *Journal of the Geological Society*, 132:17–26, 1976.

[4] Mario L. Amsler and Marcelo H. Garcia. Discussion: Sand-dune geometry of large rivers during floods. *Journal of of Hydraulic Engineering*, 123:582–585, June 1997.

[5] V. S. Shastri Annambhotla, William W. Sayre, and Robert H. Livesey. Statistical properties of Missouri River bed forms. *Journal of the Waterways, Harbors and Coastal Engineering Division*, 98(4):489–510, November 1972.

[6] Gail M. Ashley. Classification of large-scale subaqueous bedforms: a new look at an old problem. *Journal of Sedimentary Petrology*, 60(1):160–172, January 1990.

[7] Jaco A. Baas. An empirical model for the development and equilibrium morphology of current ripples in fine sand. *Sedimentology*, 46:123–138, 1999.

[8] S. J. Bennett and J. L. Best. Mean flow and turbulence structure over fixed ripples and the ripple-dune transition. In *Coherent Flow Structures in Open Channels, edited by P. J. Ashworth et al.*, number 281-304. John Wiley, 1996.

[9] J. L. Best. The fluid dynamics of small-scale alluvial bedforms. In *Advances in Fluvial Dynamics and Stratigraphy, edited by P. A. Carling and M. R. Dawson*, number 67-125. John Wiley and Sons, 1996.

[10] Jim Best. The fluid dynamics of river dunes: A review and some future research directions. *Journal of Geophysical Research*, 110, 2005.

[11] Astrid Blom and Maarten G. Kleinhans. Estimating bed form height from sorting preserved in sedimentary records of river dunes, deltas and bars. In *5th IAHR Sympo-*

sium on River, Coastal and Estuarine Morphodynamics, pages 641–648, Enschede, NL, September 2007. International Association of Hydro-Environment Research.

[12] Astrid Blom and Gary Parker. Vertical sorting and the morphodynamics of bed form-dominated rivers: a modeling framework. *Journal of Geophysical Research*, 109, 2004.

[13] John Bridge and Robert Demicco. *Earth Surface Processes, Landforms and Sediment Deposits*. Cambridge University Press, New York, USA, 2008.

[14] M. Bayani Cardenas and J. L. Wilson. The influence of ambient groundwater discharge on exchange zones induced by currentbedform interactions. *Journal of Hydrology*, 331:103–109, 2006.

[15] M. Bayani Cardenas, J. L. Wilson, and V. A. Zlotnik. Impact of heterogeneity, bed forms, and stream curvature on subchannel hyporheic exchange. *Water Resources Research*, 40, 2004.

[16] M. Bayani Cardenas, J. L. Wilson, and V. A. Zlotnik. Hydrodynamics of coupled flow above and below a sediment-water interface with triangular bedforms. *Advances in Water Resources*, 30:301–313, 2007.

[17] Y. Catano-Lopera, J. D. Abad, and M. H. Garcia. Characterization of bedform morphology generated under combined flows and currents using wavelet analysis. *Journal of Ocean Engineering*, 36:617–632, July 2009.

[18] S. E. Coleman and V. I. Nikora. Fluvial dunes: initiation, characterization, flow structure. *Earth Surface Processes and Landforms*, 36:39–57, 2011.

[19] Yadolah Dodge. *The concise encyclopedia of statistics*. Springer, New York, USA, 2008.

[20] M. Elhakeem and J. Imran. A bedload model for uniform sediment derived from the movement of bedforms. In *River, Coastal and Estuarine Morphodynamics: RCEM 2005*, pages 853–860. Taylor and Francis Group, London, 2006.

[21] Frank Engelund and Jorgen Fredsøe. Sediment ripples and dunes. *Annu. Rev. Fluid Mechanics*, 14:13–37, 1982.

[22] M. Felix, S. Sturton, and J. Peakall. Combined measurements of velocity and concentration in experimental turbidity currents. *Sedimentary Geology*, 179:31–47, 2005.

[23] Efi Foufoula-Georgiou and Praveen Kumar. *Wavelets in Geophysics*. Academic Press, Inc., USA, 1994.

[24] Sharon Gabel. Geometry and kinematics of dunes during steady and unsteady flows in the Calamus River, Nebraska, USA. *Sedimentology*, 40:237–269, 1993.

[25] Damien Garcia. Robust smoothing of gridded data in one and higher dimensions with missing values. *Computational Statistics and Data Analysis*, 54(4):1167–1178, 2010.

[26] S. Giri, S. van Vuren, W. Ottevanger, and K. Sloff. A preliminary analysis of bedform evolution in the Waal during 2002-2003 flood event using Delft3D. In *Proceedings of Marine Sandwave and River Dune Dynamics III*. School of Earth and Environment, University of Leeds, April 2008.

[27] Avijit Gupta. *Large rivers: geomorphology and management*. John Wiley, 2007.

[28] H. P. Guy, D. B. Simons, and E. V. Richardson. Summary of alluvial channel data from flume experiments, 1956-61. Prof. Paper 462-I. Technical report, U.S. Geological Survey, 1966.

[29] Muhammad I. Haque and Khalid Mahmood. Geometry of ripples and dunes. *Journal of Hydraulic Engineering*, 111(1):48–63, January 1985.

[30] Muhammad I. Haque and Khalid Mahmood. Analytical study on steepness of ripples and dunes. *Hydraulic Engineering*, 112(3):220–236, March 1986.

[31] Muhammad I. Haque and Khalid Mahmood. Sediment convection-diffusion and bedform length. *Journal of Hydraulic Engineering*, 113(11):1381–1401, November 1987.

[32] Robert R. Jr. Holmes and Marcelo H. Garcia. Flow over bedforms in a large sand-bed river: a field investigation. *Journal of Hydraulic Research*, 46(3):322–333, 2008.

[33] Roscoe G. Jackson. Largescale ripples of the lower Wabash River. *Sedimentology*, 23:593–623, 1976.

[34] Rober B. Jacobson and David L. Galat. Flow and form in rehabilitation of large-river ecosystems: an example from the Lower Missouri River. *Geomorphology*, 77:249–269, 2006.

[35] C. S. Jain and J. F. Kennedy. The growth of sand waves. In *International Symposium on Stochastic Hydraulics*. University of Pittsburgh School of Engineering Publication Series, 1971.

[36] D. J. Jerolmack, D. Mohrig, and B. McElroy. A unified description of ripples and dunes in rivers. In *River, Coastal and Estuarine Morphodynamics: RCEM 2005*, pages 843–851. Taylor and Francis Group London, 2006.

[37] Douglas Jerolmack and David Mohrig. Interactions between bed forms: Topography, turbulence, and transport. *Journal of Geophysical Research*, 110, June 2005. doi:10.1029/2004JF000126.

[38] C. M. Jones. Effects of varying discharge regimes on bed-form sedimentary structures in modern rivers. *Geology*, 5:567–570, 1977.

[39] Perre Y. Julien and Gerit J. Klaasen. Sand-dune geometry of large rivers during floods. *Journal of Hydraulic Engineering*, 121(9):657–663, September 1995.

[40] Masoud Karbasi, Mohammad H. Omid, and Javad Farhoudi. Experimental investigation of cluster bed-form formation over uniform sediment. *American Journal of Applied Sciences*, 7(8):1093–1099, 2010.

[41] Fazle Karim. Bed-form geometry in sand-bed flows. *Journal of Hydraulic Engineering*, 125:1253–1261, 1999.

[42] Philip R. Kaufmann, Jhon M. Faustini, David P. Larsen, and Mostafa A. Shirazi. A roughness-corrected index of relative bed stability for regional stream surveys. *Journal of Geomorphology*, 99:150–170, 2008.

[43] C. J. Keylock, D. R. Parsons R. D. Hardy, R. I. Ferguson, S. N. Lane, and K. S. Richards. The theoretical foundations and potential for large-eddy simulation (LES) in fluvial geomorphic and sedimentological research. *Earth-Science Reviews*, 71:271–304, 2005.

[44] K. Kheiashy, J. McCorquodale, I. Georgiou, and E. Meselhe. Geometric and statistical characteristics of bed forms in the lower Mississippi River. In *Sixth International Symposium on Coastal Engineering and Science of Coastal Sediment Process*, New Orleans, Louisiana, USA, May 2007. American Society of Civil Engineers.

[45] M. A. F. Knaapen. Local variation in the shape of superimposed bedforms as a function of local bathymetry. In *Proceedings of Marine Sandwave and River Dune Dynamics III*. School of Earth and Environment, University of Leeds, April 2008.

[46] Natalia Komarova and Alan Newell. Nonlinear dynamics of sand banks and sand waves. *Journal of Fluid Mechanics*, 415:285–321, 2000.

[47] Ray Kostaschuk. Sediment transport mechanics and subaqueous dune morphology. In *River, Coastal and Estuarine Morphodynamics: RCEM 2005*, pages 795–801. Taylor and Francis Group, London, 2006.

[48] R. A. Kuhnle, J. K. Horton, S. J. Bennett, and J. L. Best. Bed forms in bimodal sand-gravel sediments: laboratory and field analysis. *Sedimentology*, 40:631–654, 2006.

[49] David Labat. Recent advances in wavelet analyses: Part 1. A review of concepts. *Journal of Hydrology*, 314:275–288, 2005.

[50] Suzanne Leclair. Preservation of cross-strata due to the migration of subaqueous dunes: an experimental investigation. *Sedimentology*, 49:1157–1180, 2002.

[51] Raymond A. Levey, Böjrn Kjerfve, and Rufus T. Getzen. Comparison of bed form variance spectra within a meander bed during flood and average discharge. *Journal of Sedimentary Petrology*, 50(1):149–155, March 1980.

[52] Sarah Little. Wavelet analysis of seafloor bathymetry: an example. *Wavelets in Geophysics*, 4:167–182, 1994.

[53] T. B. Maddux, S. R. McLean, and J. M. Nelson. Turbulent flow over three-dimensional dunes: 2. Fluid and bed stresses. *Journal of Geophysical Research*, 108:1–171, 2003.

[54] J. R. Moll, T. Schilperoort, and A. J. De Leeuw. Stochastic analysis of bedform dimensions. *Journal of Hydraulic Research*, 25(4):465–479, 1987.

[55] Sarah. A. Morley, Jeffrey J. Duda, Holly J. Coe, Kristopher K. Kloehn, and Michael L. McHenry. Benthic invertebrates and periphyton in the Elwha River Basin: current conditions and predicted response to dam removal. *Northwest Science*, 82:179–195, 2008.

[56] Elise Mostacci, Caroline Truntzer, Harvé Cardot, and Patrick Ducoroy. Multivariate denoising methods combining wavelets and principal component analysis for mass spectrometry. *Proteomics*, 10:2564–2572, 2010.

[57] Jonathan M. Nelson, Stephen R. McLean, and Stephen R. Wolfe. Mean flow and turbulence fields over two-dimensional bed forms. *Water Resources Research*, 29:3935–3953, 1993.

[58] Vladimir I. Nikora, Alexander N. Sukhodolov, and Pawel M. Rowinski. Statistical sand wave dynamics in one-directional water flows. *Journal of Fluid Mechanics*, 351:17–39, 1997.

[59] NIST/SEMATECH. *e-Handbook of Statistical Methods*. NIST, http://www.itl.nist.gov/div898/handbook/, 2010.

[60] C. F. Nordin and J. H. Algert. Spectral analysis of sand waves. *Proc. Am. Soc. Civil Engineers*, 92:95–114, 1966.

[61] Carl F. Jr. Nordin. A stationary Gaussian model of sand waves. In *International Symposium on Stochastic Hydraulics*. University of Pittsburgh School of Engineering Publication Series, 1971.

[62] Annie Nyander, Paul S. Addison, Ian McEwan, and Gareth Pender. Analysis of river bed surface roughnesses using 2D wavelet transform-based methods. *The Arabian Journal for Science and Engineering*, 28(1C):107–121, 2003.

[63] O. Orfeo and J. Stevaux. Hydraulic and morphological characteristics of middle and upper reaches of the Paraná River (Argentina and Brazil). *Geomorphology*, 44:309–322, 2002.

[64] Aaron I. Packman, Mashfiqus Selehin, and Mattia Zaramella. Hyporheic exchange with gravel bed: basic hydrodynamic interactions and bedform-induced advective flows. *Journal of Hydraulic Engineering*, 130(7):647–656, 2004.

[65] D. R. Parsons, J. L. Best, O. Orfeo, R. J. Hardy, R. Kostaschuk, and S. N. Lane. Morphology and flow fields of three-dimensional dunes, Rio Parana, Argentina: Results

from simultaneous multibeam echo sounding and acoustic doppler current profiling. *Journal of Geophysical Research*, 110, 2005.

[66] Mariette T. H. Prent and Edward J. Hickin. Annual regime of bedforms, roughness and flow resistance, Lillooet River, British Columbia, BC. *Geomorphology*, 41:369–390, 2002.

[67] J. Raja, B. Muralikrishnan, and Shengyu Fu. Recent advances in separation of roughness, waviness and form. *Precision Engineering*, 26:222–235, 2002.

[68] André Robert and William Uhlman. An experimental study on the ripple-dune transition. *Earth Surface Processes and Landforms*, 26:615–629, 2001.

[69] A. Rossi, N. Massei, B. Laignel, D. Sebag, and Y. Copard. The response of the Mississippi River to climate fluctuations and reservoir construction as indicated by wavelet analysis of streamflow and suspended-sediment load, 19501975. *Journal of Hydrology*, 377(3-4):237–244, 2009.

[70] Dan H. Shugar, Ray Kostaschuk, James L. Best, Daniel R. Parsons, Stuart N. Lane, Oscar Orfeo, and Richard J. Hardy. On the relationship between flow and suspended sediment transport over the crest of a sand dune, Río Paraná, Argentina, journal = Sedimentology, year = 2010, optkey = , volume = 57, optnumber = , pages = 252-272, optmonth = , optnote = , optannote = .

[71] Arvind Singh, Kurt Fienberg, Douglas J. Jerolmack, and Jeffrey Marr. Experimental evidence for statistical scaling and intermittent in sediment transport rates. *Journal of Geophysical Research*, 114, 2009.

[72] T. Stoesser, C. Braun, M. García-Villalba, and W. Rodi. Turbulence structures in flow over two-dimensional dunes. *Journal of Hydraulic Engineering*, 134:42–55, 2008.

[73] Alice M. Takeda, Jose Stevaux, and Daniele S. Fujita. Effect of hydraulics, bedload grain size and water factors on habitat and abundance of narapa bonettoi righi and varela, 1983 of the upper parana river, brazil. *Hydrobiologia*, 463:241–248, 2001.

[74] Kunio Takezawa. *Introduction to Nonparametric Regression*. John Wiley and Sons, New Jersey, USA, 2006.

[75] C. Torrence and G. P. Compo. A practical guide to wavelet analysis. *Bulletin of the American Meteorological Society*, 79:61–78, 1998.

[76] A. P. Tuijnder and J. S. Ribberink. Prediction of bedform dimensions, bed roughness and sediment transport under supply-limited conditions in rivers. Technical report, Faculty of Engineering Technology, University of Twente, The Netherlands, 2009.

[77] C. F. van der Mark and A. Blom. A new and widely applicable bedform tracking tool. Technical report, University of Twente, Faculty of Engineering Technology, Department of Water Engineering and Management, March 2007.

[78] C. F. van der Mark, A. Blom, and J. M. H. Hulscher. Variability of bedform characteristics using flume and river data. In *River, Coastal and Estuarine Morphodynamics: RCEM 2007*, pages 923–930. Taylor and Francis Group, London, 2008.

[79] C. F. van der Mark, A. Blom, J. M. H. Hulscher, S. F. Leclair, and D. Mohrig. On the modeling the variability of bedform dimensions. In *River, Coastal and Estuarine Morphodynamics: RCEM 2005*, pages 831–841. Taylor and Francis Group, London, 2006.

[80] C. F. van der Mark, A. Blom, and J. S. M. Hulscher. Quantification of variability in bedform geometry. *Journal of Geophysical Research*, 113, 2008.

[81] Jeremy G. Venditti, Michael Church, and Sean J. Bennett. On the transition between 2D and 3D dunes. *Sedimentology*, 52:1343–1359, 2005.

[82] Zhi-Qian Wang and Nian-Sheng Cheng. Time-mean structure of secondary flows in open channel with longitudinal bedforms. *Advances in Water Resources*, 29:1634–1649, 2006.

[83] J. J. Warmink, M. J. Booij, S. J. M. H. Hulscher, and H. Van der Klis. Uncertainty in design water levels due to uncertain bed form roughness in the River Rhine. In *International Conference on Fluvial Hydraulics (River Flow 2010)*, pages 359–366, Braunschweig, Germany, September 2010. IAHR - Fluvial Hydraulics Committee, Technische Universität Braunschweig, EWE Aktiengesellschaft.

[84] Mark L. Wildhaber, Peter J. Lamberson, and David L. Galat. A comparison of measures of riverbed form for evaluating distributions of benthic fishes. *North American Journal of Fisheries Management*, 23:543–557, 2003.

[85] Salim Yalin and Grace Lai. On the form drag caused by sand waves. Technical Report 363/II-4, Japan Society of Civil Engineers, November 1985.